This is the accepted manuscript made available via CHORUS. The article has been published as:

Multiband s-wave topological superconductors: Role of dimensionality and magnetic field response

Shusa Deng, Gerardo Ortiz, and Lorenza Viola

Phys. Rev. B **87**, 205414 — Published 8 May 2013

DOI: 10.1103/PhysRevB.87.205414

Multiband s-wave topological superconductors: role of dimensionality and magnetic field response

Shusa Deng,[1] Gerardo Ortiz,[2] and Lorenza Viola[1]

[1] *Department of Physics and Astronomy, Dartmouth College, Hanover, New Hampshire 03755, USA*
[2] *Department of Physics, Indiana University, Bloomington, Indiana 47405, USA*

We further investigate a class of time-reversal-invariant two-band s-wave topological superconductors introduced in Phys. Rev. Lett. **108**, 036803 (2012). Provided that a *sign reversal* between the two superconducting pairing gaps is realized, the topological phase diagram can be determined exactly (within mean field) in one and two dimensions, as well as in three dimensions upon restricting to the excitation spectrum of time-reversal invariant momentum modes. We show how, in the presence of time-reversal symmetry, $\mathbb{Z}_2$ invariants that distinguish between trivial and non-trivial quantum phases can be constructed by considering *only one* of the Kramers' sectors in which the Hamiltonian decouples into. We find that the main features identified in our original two-dimensional setting remain qualitatively unchanged, with non-trivial topological superconducting phases supporting an *odd number of Kramers' pairs* of helical Majorana modes on each boundary, as long as the required π phase difference between gaps is maintained. We also analyze the consequences of time-reversal symmetry-breaking either due to the presence of an applied or impurity magnetic field or to a deviation from the intended phase matching between the superconducting gaps. We demonstrate how the relevant notion of topological invariance must be modified when time-reversal symmetry is broken, and how both the persistence of gapless Majorana modes and their robustness properties depend in general upon the way in which the original Hamiltonian is perturbed. Interestingly, a topological quantum phase transition between helical and chiral superconducting phases can be induced by suitably tuning a Zeeman field in conjunction with a phase mismatch between the gaps. Recent experiments in doped semiconducting crystals, of potential relevance to the proposed model, and possible candidate material realizations in superconductors with $s_\pm$ pairing symmetry are discussed.

PACS numbers: 73.20.At, 74.78.-w, 71.10.Pm, 03.67.Lx

I. INTRODUCTION

Obtaining a complete understanding of topological quantum matter has a fundamental significance across condensed-matter physics as well as potential practical implications within quantum science. On the one hand, characterizing "non-local" topological order and unveiling connections with the emergence of "topologically protected" edge states are prerequisites for developing a unified classification of matter beyond Landau's paradigm of symmetry breaking[1]. On the other hand, taking full advantage of the distinctive robustness features that the degenerate ground-state manifold enjoys may offer new pathways to fault-tolerance in topological quantum memory and quantum computation[2,3].

Building on the paradigmatic example of quantum Hall liquids and the recent discovery of topological insulators[3–5] (TIs), *topological superconductors*[6–9] (TSs) are attracting a growing theoretical and experimental interest in this context. TSs are gapped phases of fermionic quantum matter whose "zero-energy" edge states are naturally associated to *Majorana quasi-particles*, that is, fermions which are their own antiparticle, as originally suggested by Ettore Majorana back in 1937[10]. Remarkably, Majorana exchange operations may lead, under appropriate conditions, to non-Abelian statistics[7,11,12], making Majorana states uniquely suited in principle to both fundamental quantum studies and topological qubit implementations. As a result, a variety of proposals have been put forward in recent years to engineer Majorana fermions in different condensed-matter platforms.

A number of proposed TS realizations involve explicit breaking of time-reversal (TR) symmetry – notably, the seminal "Kitaev's wire" in one dimension (1D)[8] and the chiral superconductors with $p + ip$ pairing symmetry[6], as well as subsequent 1D hybrid semiconductor-superconductor nano-wires as well as heterostructures in 2D, see Refs. 13–19 for representative contributions. Our interest, however, is in *TR-invariant topological superconductivity*. Existing proposals for TR-invariant TSs have thus far largely relied on the proximity effect between a 3D TI and a conventional (s-wave) superconductor[20,21] (see also Ref. 22 for early contributions), or on access to unconventional ($p + ip$ and/or spin-triplet) superconducting order parameter[23–25].

Our motivation is to explore whether alternative routes to TR-invariant TSs exist based on conventional s-wave bulk pairing symmetry. Our key physical insight is to take advantage of *multiband* superconductivity, directly in the spirit of the original proposal by Suhl-Matthias-Walker (SMW) for two-band s-wave superconductors[26]. Following the experimental discovery of MgB_2 in 2001[27], signatures of multi-band superconductivity have been reported by now for a variety of materials[28], including newly discovered iron-based superconductors[29]. A model Hamiltonian for a 2D TR-invariant centro-symmetric two-band s-wave TS supporting Majorana edge states was proposed in Ref. 30, under the condition that a *sign*

reversal be enforced between the two pairing gaps. From a mathematical viewpoint, such a two-band model can equally describe a bi-layer system where the band index is replaced by a layer index[30–33]. In this work, we aim to continue our exploration of TR-invariant multi-band TS, with the goal of (i) obtaining a more complete characterization of the non-trivial topological features that emerge for this class of Hamiltonians; and (ii) gaining a deeper insight on basic aspects of TS and their edge states in general. The content is organized as follows.

We begin in Sec. II by introducing the relevant class of two-band TR-invariant model Hamiltonians for systems of different spatial dimension. While it is not possible to analytically determine the excitation spectrum for general parameter values, we show how an *exact* solution leading to non-trivial topological behavior may be obtained under the assumption that the two *pairing gaps are π-shifted* from one another, including in 3D as long as we focus on the excitation spectrum of TR-invariant modes. We argue that, as long as two decoupled "Kramers' sectors" are identifiable, restricting to a *single* such sectors allows to naturally construct $\mathbb{Z}_2$ topological invariants applicable when TR symmetry is preserved. In particular, we demonstrate how topological numbers originally defined in low dimension (such as, notably, Berry phases) can be extended beyond 1D upon restriction to low-dimensional manifolds in parameter space.

Section III is devoted to characterizing the topological features that emerge in our model as the spatial dimension increases from 1D to 3D. This is done by first examining the bulk topological response, and then by establishing the extent to which bulk properties relate to the existence of Majorana edge states via a bulk-boundary correspondence. In all dimensions, we find that a $\mathbb{Z}_2$ invariant distinguishes topologically trivial from non-trivial TS phases. The latter are found to support an *odd number of Kramers' pairs of counter-propagating (helical) Majorana modes on each boundary*. We explicitly show that gapless Majorana modes existing in topologically trivial phases are generally not robust against perturbations, even if TR-symmetry is preserved.

In Sec. IV, we explore the consequences of explicitly breaking TR according to different mechanisms, with emphasis on determining the conditions under which gapless Majorana modes may persist, and characterizing their degree of robustness compared to the TR-invariant case. We first analyze the effect of a static magnetic field in various physical scenarios, allowing for the field to act in different directions on the bulk or solely on the boundary, respectively. In particular, we show how the *full* excitation spectrum can still be exactly determined in the presence of a longitudinal Zeeman field in 2D, and how topological invariants must be appropriately redefined as a consequence of TR symmetry being broken. In general, we find that gapless Majorana modes may exist in the presence of applied or impurity magnetic fields. However, *their degree of robustness against subsequent perturbations depends in general on both the symmetry and the details of the latter*. Similar conclusions apply if TR symmetry is explicitly broken due to a phase mismatch between the pairing gaps relative to the intended value of π. Remarkably, the application of a suitable Zeeman field may then be used to *restore gapless Majorana modes* that would be gapped in under a phase mismatch alone, and to induce a topological quantum phase transition (QPT) between helical and chiral phases, accompanied by a vanishing bulk gap.

In Sec. V, we present some considerations on the practical feasibility of our proposal in real materials. In particular, we qualitatively discuss implications in the context of the search for topological superconductivity in 3D doped TI materials[34–36], and follow up on our original suggestion[30] of realizations in iron-based superconductors exhibiting *$s_\pm$ pairing symmetry*. We conclude in Sec. VI with a summary of our main results and an outlook to open problems. Additional technical details are included in the Appendices. Specifically, Appendix A presents a complete symmetry analysis of our TS model Hamiltonian, thereby defining its symmetry class. Appendix B briefly discusses the role of the self-consistency constraint in determining the physical accessibility and stability of different phases, whereas Appendix C shows the explicit form of the Hamiltonian matrix when arbitrary static magnetic fields perturb the TS system. Finally, Appendix D addresses the important problem of a consistent, numerically gauge-invariant evaluation of topological invariants, by discussing Berry phase and Chern number computations.

II. TIME-REVERSAL INVARIANT TOPOLOGICAL SUPERCONDUCTORS

A. Model Hamiltonian

Our starting point is a class of TR-invariant two-band Hamiltonians of the form introduced in Ref. 30. Consider a regular lattice in D spatial dimensions, with orthonormal vectors $\{\hat{e}_\nu \,|\, \nu \in u_D\} \equiv \{\hat{x}, \hat{y}, \hat{z}, \ldots\}$, where the relevant set of indexes u_D depends upon dimensionality and N_ν is the number of lattice sites in the νth direction (for example, $u_2 = \{x, y\}$ with a total number of sites $N = N_x N_y$ in 2D, and so on). Let c and d label two orbitals (bands) and for each lattice site j introduce

$$\psi_j \equiv (c_{j,\uparrow}, c_{j,\downarrow}, d_{j,\uparrow}, d_{j,\downarrow})^T,$$

in terms of fermionic annihilation operators $c_{j,\sigma}, d_{j\sigma}$, with $\sigma = \uparrow, \downarrow$ denoting the spin quantum number. Let us also introduce Pauli matrices τ_ν and σ_ν ($\nu = x, y, z$) that act on the orbital and spin part, respectively. Then the relevant Hamiltonian may be written as

$$H_D = H_{\mathsf{cd}} + H_{\mathsf{so}} + H_{\mathsf{sw}} + \text{H.c.}, \tag{1}$$

where the different terms have the following expression:

$$\begin{aligned} H_{\mathsf{cd}} &= \frac{1}{2}\sum_j (u_{cd}\psi_j^\dagger \tau_x \psi_j - \mu\psi_j^\dagger\psi_j) - t\sum_{\langle i,j\rangle}\psi_i^\dagger\tau_x\psi_j, \\ H_{\mathsf{so}} &= i\lambda\sum_{j,\nu\in u_D}\psi_j^\dagger\tau_z\sigma_\nu\psi_{j+\hat{e}_\nu}, \\ H_{\mathsf{sw}} &= \sum_j(\Delta_c c_{j,\uparrow}^\dagger c_{j,\downarrow}^\dagger + \Delta_d d_{j,\uparrow}^\dagger d_{j,\downarrow}^\dagger). \end{aligned} \quad (2)$$

Physically, H_{cd}, H_{so}, and H_{sw} represents the two-band internal dynamics, the spin-orbit (SO) interaction, and the s-wave intra-band superconducting fluctuations, respectively. The parameter μ is the chemical potential, u_{cd} is an on-site spin-independent hybridization term between the two bands, whereas t quantifies the strength of inter-band hopping, with $\langle i,j\rangle$ representing nearest-neighbor sites i and j. Note that, for simplicity, we have assumed here that no inter-band SO coupling is present and, without loss of generality, we have taken the strength of the SO coupling to be the same, equal to λ, for each band. The parameters Δ_c and Δ_d represent the s-wave pairing gaps of the two bands within the mean-field approximation, that is, in momentum space,

$$\Delta_c = -V_{cc}\langle c_{\mathbf{k},\uparrow}c_{-\mathbf{k},\downarrow}\rangle, \quad \Delta_d = -V_{dd}\langle d_{\mathbf{k},\uparrow}d_{-\mathbf{k},\downarrow}\rangle, \quad (3)$$

with $V_{cc} > 0$, $V_{dd} > 0$ being the effective attraction strength for fermions in each band[26].

Notice that in the limit where $\mu = 0$ and no superconducting fluctuations are present, $H_{\mathsf{sw}} = 0$, the Hamiltonian H_D in Eq. (1) reduces to the so-called Dimmock model for a TI[37,38]. From the point of view of the symmetry classification introduced by Altland and Zirnbauer[39], one may explicitly verify (see Appendix A) that H_D exhibits manifest invariance under both TR and particle-hole (PH) transformations, in addition to exhibiting inversion symmetry, indicating that the model can be taken to belong to DIII symmetry class. In particular, TR symmetry constrains each of the mean-field pairing gaps to be real, with a phase equal to 0 or π.

For general parameter values and periodic boundary conditions (PBC), H_D can be block-diagonalized by a Fourier transformation in all spatial directions. That is, we may rewrite

$$H_D = \frac{1}{2}\sum_{\mathbf{k}}(\hat{A}_{\mathbf{k}}^\dagger \hat{H}_{\mathbf{k}}\hat{A}_{\mathbf{k}} - 4\mu), \quad (4)$$

where

$$\hat{A}_{\mathbf{k}}^\dagger = (c_{\mathbf{k},\uparrow}^\dagger, c_{\mathbf{k},\downarrow}^\dagger, d_{\mathbf{k},\uparrow}^\dagger, d_{\mathbf{k},\downarrow}^\dagger, c_{-\mathbf{k},\uparrow}, c_{-\mathbf{k},\downarrow}, d_{-\mathbf{k},\uparrow}, d_{-\mathbf{k},\downarrow}),$$

and $\hat{H}_{\mathbf{k}}$ is a 8×8 matrix in general:

$$\hat{H}_{\mathbf{k}} = \begin{pmatrix} -\mu+\vec{\lambda}_{\mathbf{k}}\cdot\vec{\sigma} & m_{\mathbf{k}} & i\Delta_c\sigma_y & 0 \\ m_{\mathbf{k}} & -\mu-\vec{\lambda}_{\mathbf{k}}\cdot\vec{\sigma} & 0 & i\Delta_d\sigma_y \\ -i\Delta_c\sigma_y & 0 & \mu+\vec{\lambda}_{\mathbf{k}}\cdot\vec{\sigma}^* & -m_{\mathbf{k}} \\ 0 & -i\Delta_d\sigma_y & -m_{\mathbf{k}} & \mu-\vec{\lambda}_{\mathbf{k}}\cdot\vec{\sigma}^* \end{pmatrix}. \quad (5)$$

Here, * denotes complex conjugation and we have introduced the compact notations

$$\begin{cases} \vec{\lambda}_{\mathbf{k}} \equiv -2\lambda\sum_{\nu\in u_D}\sin k_\nu\,\hat{e}_\nu, \\ m_{\mathbf{k}} \equiv u_{cd} - 2t\sum_{\nu\in u_D}\cos k_\nu, \\ \vec{\sigma} \equiv \sum_{\nu\in u_D}\sigma_\nu\,\hat{e}_\nu. \end{cases}$$

Remarkably, an exact analytical solution exists in both 1D and 2D in the limit where the pairing gaps are π-shifted, that is,

$$\Delta_c = -\Delta_d \equiv \Delta, \quad (6)$$

in which case $\hat{H}_{\mathbf{k}}$ in Eq. (5) decouples into two 4×4 matrices. Specifically, upon introducing new canonical fermionic operators,

$$\begin{cases} a_{\mathbf{k},\sigma} = \frac{1}{\sqrt{2}}(c_{\mathbf{k},\sigma} + d_{\mathbf{k},\sigma}), \\ b_{\mathbf{k},\sigma} = \frac{1}{\sqrt{2}}(c_{\mathbf{k},\sigma} - d_{\mathbf{k},\sigma}), \end{cases} \quad (7)$$

we may rewrite

$$H_D = \frac{1}{2}\sum_{\mathbf{k}}(\hat{B}_{\mathbf{k}}^\dagger \hat{H}'_{\mathbf{k}}\hat{B}_{\mathbf{k}} - 4\mu),$$

with

$$\hat{B}_{\mathbf{k}}^\dagger = (a_{\mathbf{k},\uparrow}^\dagger, b_{\mathbf{k},\downarrow}^\dagger, a_{-\mathbf{k},\uparrow}, b_{-\mathbf{k},\downarrow}, a_{-\mathbf{k},\downarrow}^\dagger, b_{-\mathbf{k},\uparrow}^\dagger, a_{\mathbf{k},\downarrow}, b_{\mathbf{k},\uparrow}),$$

and $\hat{H}'_{\mathbf{k}} = \hat{H}'_{+,\mathbf{k}} \oplus \hat{H}'_{-,\mathbf{k}}$, where

$$\hat{H}'_{+,\mathbf{k}} = \begin{pmatrix} m_{\mathbf{k}}\sigma_z - \mu + \vec{\lambda}_{\mathbf{k}}\cdot\vec{\sigma} & i\Delta\sigma_y \\ -i\Delta\sigma_y & -m_{\mathbf{k}}\sigma_z + \mu + \vec{\lambda}_{\mathbf{k}}\cdot\vec{\sigma}^* \end{pmatrix}, \quad (8)$$

$$\hat{H}'_{-,\mathbf{k}} = \begin{pmatrix} m_{\mathbf{k}}\sigma_z - \mu - \vec{\lambda}_{\mathbf{k}}\cdot\vec{\sigma}^* & -i\Delta\sigma_y \\ i\Delta\sigma_y & -m_{\mathbf{k}}\sigma_z + \mu - \vec{\lambda}_{\mathbf{k}}\cdot\vec{\sigma} \end{pmatrix}. \quad (9)$$

Notice that the 4×4 matrices $\hat{H}'_{+,\mathbf{k}}$ and $\hat{H}'_{-,\mathbf{k}}$ may be regarded as TR of one another, in the following sense: by partitioning the fermonic operators $\hat{B}_{\mathbf{k}} \equiv \hat{B}_{+,\mathbf{k}} \oplus \hat{B}_{-,\mathbf{k}}$ and using the explicit form of the TR transformation $\mathcal{T}$ given in Appendix A, that is:

$$\mathcal{T}a(b)_{\mathbf{k},\uparrow}\mathcal{T}^{-1} = a(b)_{-\mathbf{k},\downarrow}, \;\; \mathcal{T}a^\dagger(b^\dagger)_{\mathbf{k},\downarrow}\mathcal{T}^{-1} = -a^\dagger(b^\dagger)_{-\mathbf{k},\uparrow},$$

$$\mathcal{T}a(b)_{\mathbf{k},\downarrow}\mathcal{T}^{-1} = -a(b)_{-\mathbf{k},\uparrow}, \;\; \mathcal{T}a^\dagger(b^\dagger)_{\mathbf{k},\uparrow}\mathcal{T}^{-1} = a^\dagger(b^\dagger)_{-\mathbf{k},\downarrow},$$

we may write:

$$\mathcal{T}\left(\hat{B}_{+,\mathbf{k}}^\dagger \hat{H}'_{+,\mathbf{k}}\hat{B}_{+,\mathbf{k}}\right)\mathcal{T}^{-1} = \hat{B}_{-,\mathbf{k}}^\dagger \hat{H}'_{-,\mathbf{k}}\hat{B}_{-,\mathbf{k}}.$$

The excitation spectrum obtained from diagonalizing either "Kramers' sector" $\hat{H}'_{+,\mathbf{k}}$ or $\hat{H}'_{-,\mathbf{k}}$ is given by

$$\epsilon_{n,\mathbf{k}} = \pm\sqrt{m_{\mathbf{k}}^2 + \Omega^2 + |\vec{\lambda}_{\mathbf{k}}|^2 \pm 2\sqrt{m_{\mathbf{k}}^2\Omega^2 + \mu^2|\vec{\lambda}_{\mathbf{k}}|^2}}, \quad (10)$$

where $\Omega^2 \equiv \mu^2 + \Delta^2$ and we have assumed the energy ordering $\epsilon_{1,\mathbf{k}} \leq \epsilon_{2,\mathbf{k}} \leq 0 \leq \epsilon_{3,\mathbf{k}} \leq \epsilon_{4,\mathbf{k}}$. Clearly, $\epsilon_{n,\mathbf{k}} = \epsilon_{n,-\mathbf{k}}$, as implied by inversion symmetry. QPTs occur when the gap closes, that is, $\epsilon_{2,\mathbf{k}} = 0$, for general $\Delta \neq 0$, leading to the QPT lines determined by

$$m_{\mathbf{k}_c} = \pm\,\Omega, \quad k_{\nu,c} \in \{0, \pi\},\ \nu \in u_D.$$

Note that the above condition is *independent* upon the SO strength λ, as long as $\lambda \neq 0$.

In 3D, the Hamiltonian H_D can no longer be decoupled into 4×4 matrices due to the SO coupling along the z direction (see Appendix C), implying that no analytical solution of the excitation spectrum can be obtained in general. However, since for the TR-invariant modes the gap closes only at the QCPs, and the SO coupling term vanishes for the TR-invariant modes, that is, for $k_{\nu,c} \in \{0, \pi\}$, $\nu \in u_D$, we may focus on the excitation spectrum for $k_z = k_{z,c}$. In this case, the decoupled structure into two TR Hamiltonians $\hat{H}'_{\pm,\mathbf{k}}$ still holds, and thus we obtain exactly the same form of excitation spectrum as in Eq. (10) for the corresponding energies $\epsilon_{n,\mathbf{k}=(k_x,k_y,k_{z,c})}$. The phase diagram of the Hamiltonian H_D, as the dimension changes from 1D to 3D, will be discussed in detail in Sec. III, with appropriate topological numbers being identified and labeling each phase.

Two additional remarks are in order in regard to the Hamiltonian H_D in Eqs. (1)-(2). First, the contribution H_{sw} is a *special case* of the general SMW Hamiltonian for a two-band superconductor with s-wave pairing symmetry[26], corresponding to the situation where no inter-band electron-phonon process takes place. In this case, the two superconducting gaps are also associated with two distinct transition temperatures. In principle (and in fact most likely in real materials), an inter-band interaction Hamiltonian of the form

$$H_{\mathsf{cd}} = -\sum_{\mathbf{k},\mathbf{k}'} V_{cd}(c^\dagger_{\mathbf{k},\uparrow} c^\dagger_{-\mathbf{k},\downarrow} d_{-\mathbf{k}',\downarrow} d_{\mathbf{k}',\uparrow} + \text{H.c.}),\ V_{cd} > 0,$$

may also be present, in addition to the two intra-band interactions with strength V_{cc} and V_{dd} in Eqs. (2)-(3). Within a mean-field description, it is easy to check that the effect of the additional term amounts to a renormalization of the attraction strengths for each band,

$$\Delta_c \mapsto \Delta'_c \equiv V_{cc}\Delta_c + V_{cd}\Delta_d,$$
$$\Delta_d \mapsto \Delta'_d \equiv V_{cd}\Delta_c + V_{dd}\Delta_d.$$

Thus, our analysis can be straightforwardly extended to the general case $V_{cd} \neq 0$. In particular, requiring that $\Delta'_c = -\Delta'_d$ still yields $\Delta_c = -\Delta_d$ as a unique solution if $V_{cc} = V_{dd}$, therefore all the results obtained for $V_{cd} = 0$ apply with no modification in this case. While different attraction strengths, as determined by band structure details, can be easily accommodated in principle, we shall show in Sec. IV B that the specific values of these parameters do not play a crucial role (cf. Fig. 10). Thus, for simplicity we shall focus on the already rich behavior emerging for $V_{cc} = V_{dd}$ henceforth.

Second, as written in Eq. (2), the superconducting term in H_D involves s-wave pairing *in each band* separately. Consider, however, the following unitary transformation for each mode $\mathbf{k}$:

$$U = \frac{1}{\sqrt{2}}\Big\{ I_{2\times 2} \otimes \Big[(\sigma_x + \sigma_z) \otimes I_{2\times 2}\Big]\Big\}.$$

Then, at the symmetry point defined by Eq. (6), H_D transforms into:

$$\tilde{H}_D = \frac{1}{2}\sum_{\mathbf{k}} [\hat{A}^\dagger_{\mathbf{k}}(U\hat{H}_{\mathbf{k}}U^\dagger)\hat{A}_{\mathbf{k}} - 4\mu],$$

which can in turn be written in real space as follows:

$$\begin{aligned}\tilde{H}_D \;=\; & \frac{1}{2}\sum_j (u_{cd}\psi^\dagger_j \tau_z \psi_j - \mu\psi^\dagger_j\psi_j) - t\sum_{\langle i,j\rangle}\psi^\dagger_i\tau_z\psi_j \\ & +\; i\lambda\sum_{j,\nu\in u_D}\psi^\dagger_j\tau_x\sigma_\nu\psi_{j+\hat{e}_\nu} \\ & +\; \sum_j \Delta(c^\dagger_{j,\uparrow}d^\dagger_{j,\downarrow} - c^\dagger_{j,\downarrow}d^\dagger_{j,\uparrow}) + \text{H.}c., \end{aligned} \tag{11}$$

That is, the original intra-band superconductivity is transformed into *inter-band spin-singlet superconductivity*, with the original intra-band SO interaction being correspondingly transformed into inter-band SO interaction. Thus, all the results obtained from investigating H_D in the limit $\Delta_c = -\Delta_d$ can be directly generalized to the class of models described by $\tilde{H}_D$.

B. Topological Indicators

Since the Hamiltonian H_D preserves TR symmetry, topological invariants that are applicable to the TR-broken case will, in general, fail to characterize the system's topological response. While different approaches have been pursued[20,40–42], our strategy is to build on previous work[43,44] and construct suitable "partial" topological quantum numbers in order to distinguish between topologically trivial and non-trivial phases[30]. In particular, in this work we shall focus on three kinds of topological indicators, which we define in what follows. We anticipate that despite their different form, these indicators are in essence equivalent when applicable, as we will demonstrate for our system in Sec. III.

• **Partial Berry phase sum parity.** Consider the simplest 1D case first. By taking advantage of the decoupled structure between TR-pairs in the limit of π-shifted gaps [Eq. (6)], we may consider the sum of the Berry phases[43–45] for the *two occupied negative bands of one Kramers' sector only*, say, $|\psi_{1,k_x}\rangle$ and $|\psi_{2,k_x}\rangle$ of $\hat{H}'_{+,\mathbf{k}}$, with each Berry phase given by (see also Appendix D for more detail on the actual numerical calculation):

$$B_n = i\int_{-\pi}^{\pi} dk_x \langle\psi_{n,k_x}|\partial_{k_x}\psi_{n,k_x}\rangle. \tag{12}$$

Since B_n may only attain the values 0 or π (mod 2π) for a system with inversion symmetry[46], a $\mathbb{Z}_2$ topological invariant may be naturally constructed as follows:

$$P_B = (-1)^{\mathrm{mod}_{2\pi}(B_+)/\pi}, \;\; B_+ \equiv B_1 + B_2. \tag{13}$$

For $D > 1$, the basic idea is to use lower-dimensional topological numbers upon restricting to a lower-dimensional manifold in parameter space[44]. In 2D, for instance, note that the superconductor in the momentum planes $k_{y,c} \in \{0, \pi\}$ is mapped to itself under inversion and has the topology of a 1D ring under PBC. Thus, it is possible to define a $\mathbb{Z}_2$ invariant by analyzing the parity of the partial Berry phase sum *restricted to the planes* $k_y = k_{y,c}$. That is,

$$P_B = (-1)^{\mathrm{mod}_{2\pi}(B_+)/\pi}, \; B_+ = \sum_{k_y=0,\pi} (B_{k_y,1} + B_{k_y,2}). \tag{14}$$

The 3D case can be treated in a similar fashion and is discussed in more detail directly in Sec. III A 3.

• **Partial Chern sum parity.** This invariant was originally introduced and used in Ref. 30 for the 2D geometry. In a similar spirit to the above, the idea is to use the Chern numbers (CNs) of the *two occupied negative bands of one Kramers' sector only*, say $\hat{H}'_{+,\mathbf{k}}$ as before. Call these CNs C_1 and C_2, and let $|\psi_{n,\mathbf{k}}\rangle$ denote the band-n eigenvector of $\hat{H}'_{+,\mathbf{k}}$. Then the CNs $C_n \in \mathbb{Z}$, $n = 1, 2$, are given by (see also Appendix D for its numerical implementation):

$$C_n = \frac{1}{\pi} \int_{-\pi}^{\pi} dk_x \int_{-\pi}^{\pi} dk_y \, \mathrm{Im} \, \langle \partial_{k_x} \psi_{n,\mathbf{k}} | \partial_{k_y} \psi_{n,\mathbf{k}} \rangle. \tag{15}$$

Thus, a $\mathbb{Z}_2$ invariant may be constructed as follows:

$$P_C \equiv (-1)^{\mathrm{mod}_2(C_+)}, \quad C_+ \equiv C_1 + C_2. \tag{16}$$

Again, the extension to the 3D case will be addressed in Sec. III A 3.

• **Partial fermion number parity.** As discussed in Ref. 30, there is a direct connection between the invariant P_C defined in Eq. (16) and the fermion number parity of the TR-invariant modes. Let us focus on the ground-state fermion number parity of the TR-invariant points $\mathbf{k}_c$ in the first Brillouin zone. Since for these modes, the two TR Hamiltonians $\hat{H}'_{+,\mathbf{k_c}}$ and $\hat{H}'_{-,\mathbf{k_c}}$ are decoupled, we need only concentrate on the ground-state parity property of $\hat{H}'_{+,\mathbf{k_c}}$. Let us introduce the new basis given by

$$u_{\mathbf{k}_c} \equiv \{a^\dagger_{\mathbf{k}_c,\uparrow}|\mathrm{vac}\rangle, b^\dagger_{\mathbf{k}_c,\downarrow}|\mathrm{vac}\rangle, |\mathrm{vac}\rangle, a^\dagger_{\mathbf{k}_c,\uparrow} b^\dagger_{\mathbf{k}_c,\downarrow}|\mathrm{vac}\rangle\}.$$

In this basis, $\hat{H}'_{+,\mathbf{k_c}}$ becomes

$$\widehat{H}_{+,\mathbf{k}_c} = -\mu I_{4\times 4} + [m_{\mathbf{k}_c}\sigma_z \oplus (\Delta\sigma_x + \mu\sigma_z)],$$

with eigenvalues $-\mu \pm m_{\mathbf{k}_c}, -\mu \pm |\Omega|$. When $|m_{\mathbf{k}_c}| > |\Omega|$, the ground state of each mode $\mathbf{k}_c$ is in the sector with odd fermion parity, $P_{\mathbf{k}_c} = e^{i\pi(a^\dagger_{\mathbf{k}_c,\uparrow} a_{\mathbf{k}_c,\uparrow} + b^\dagger_{\mathbf{k}_c,\downarrow} b_{\mathbf{k}_c,\downarrow})} = -1$; conversely, when $|m_{\mathbf{k}_c}| < |\Omega|$, it is in the sector with even fermion parity $P_{\mathbf{k}_c} = 1$. Thus, we define a $\mathbb{Z}_2$ partial fermion number parity invariant as follows:

$$P_F = \prod_{\mathbf{k_c}} P_{\mathbf{k_c}}. \tag{17}$$

Computing the fermion number parity of the TR-invariant modes *from one representative of each Kramers' pairs* is consistent with the fact that only a partial CN (or Berry phase) sum can detect TS phases in the presence of TR symmetry.

III. ROLE OF DIMENSIONALITY

A relevant question regarding the existence of non-trivial TS phases and their physical properties is the role played by spatial dimensionality. In this section, we will explore the topological response of our Hamiltonian H_D as we move from 1D to 3D, first through *bulk properties*, that is, by computing the topological numbers from the bulk Hamiltonian; and then through the *bulk-boundary correspondence*, that is, the relationship between the nature of the bulk vacuum in the thermodynamic limit and the existence of surface modes on the boundary.

A. Bulk properties

1. Topological response in 1D

The so-called Kitaev wire[8], which is essentially the XY chain in a transverse magnetic field written in fermionic language, has attracted a lot of attention recently for supporting an odd number of Majorana modes on the boundary, as originally remarked in Ref. 47 (see also Ref. 48). Does our TR-invariant two-band TS model in 1D ($u_1 = x$) also exhibit non-trivial topological phases?

The natural choice of topological indicator is the partial Berry phase sum parity, instead of the partial Chern sum parity, which requires at least a 2D parameter space [cf. Eq. (15)]. The phase diagram obtained (for $\mu = 0$) from requiring $\epsilon_{2,\mathbf{k}_c} = 0$ is depicted in Fig. 1, where the integer numbers in square brackets are the partial Berry phase sum parity P_B, with $P_B = -1(1)$ corresponding to non-trivial (trivial) topological phases, respectively. The phase diagram shows the topological phases of the 1D Hamiltonian indexed by a $\mathbb{Z}_2$ number, as expected from general classification arguments in this simple case[39,49].

2. Topological response in 2D

In 2D, we may compute both the partial CNs [C_n, Eq. (15)] and the partial Berry phase of each occupied band [$B_{k_{y,c},n}$, Eq. (14)] by following the procedure outlined in

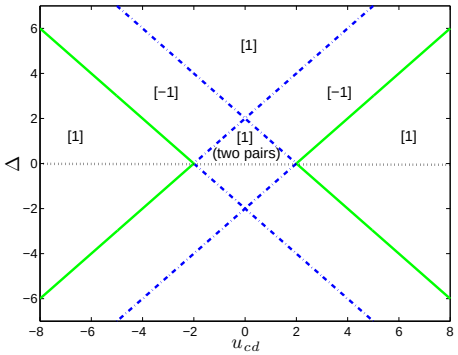

FIG. 1: (Color online) Phase diagram of the Hamiltonian H_D in 1D as a function of u_{cd} and Δ, with $t = 1 = \lambda$, for representative chemical potential $\mu = 0$. As noted, the phase diagram is independent upon λ provided that $\lambda \neq 0$. The horizontal black dotted line at $\Delta = 0$ represents an insulator or metal phase, depending on the filling. The topological response is characterized via the partial Berry phase sum parity P_B, given in square bracket. Notice that the phase diagram is symmetric under $\Delta \mapsto -\Delta$. System size: $N_x = 100$.

Appendix D. We find that the parity of the partial Berry phase sum, P_B, is consistent with the parity of partial Chern sum, P_C, in the whole parameter space.

The topological responses for $\mu = 0$ and $\mu = -1$ as representative examples are shown in the two top panels of Fig. 2, with the integer numbers in parenthesis giving the partial Chern sum C_+ [see also Fig. 1 in Ref. 30]. As it will become explicit from analyzing the bulk-boundary correspondence (Sec. III B), an odd (even) value of C_+ corresponds to non-trivial (trivial) topological phases, respectively. We stress that in 2D QPTs are present also between phases carrying the *same* partial Chern sum parity, for instance separating phases with $C_+ = 1$ and $C_+ = -1$, as well as $C_+ = 0$ and $C_+ = \pm 2$ (blue dash-dotted lines). Thus, a $\mathbb{Z}$ *invariant is necessary in order to identify all the topological phases* in the bulk phase diagram. A similar characterization was encountered for the model analyzed in Ref. 50, where, however, TR symmetry is explicitly broken. Since the partial Berry phase sum is, by definition, a $\mathbb{Z}_2$ quantity, this also makes B_+ inadequate to fully characterize the phase diagram, although P_B still correctly diagnoses the presence of non-trivial topological features.

3. *Topological response in 3D*

The 3D Hamiltonian H_D is especially interesting in the light of recent discoveries of candidate TIs[52] and investigations of possible TS materials in 3D geometries[34–36]. Since our 3D superconductor in the momentum planes $k_z = k_{z,c} \in \{0, \pi\}$ is mapped to itself under inversion and has the topology of a 2D torus under PBC, we may define a $\mathbb{Z}_2$ invariant by analyzing the partial Chern sum restricted to such planes. If $C_+^{k_{z,c}}$ denotes the corresponding partial Chern sum, then we can define the following $\mathbb{Z}_2$ parity invariant:

$$P_C \equiv (-1)^{\mathrm{mod}_2(C_+)}, \;\; C_+ \equiv C_+^0 + C_+^\pi. \tag{18}$$

Note that we could choose the partial Chern sum on the planes $k_x = k_{x,c}$ or $k_y = k_{y,c}$. It is easy to verify that the resulting values of P_C would be the same on the planes $k_x = k_{x,c}$, $k_y = k_{y,c}$, and $k_z = k_{z,c}$. In fact, since only the parity of $(C_+^0 + C_+^\pi)$ matters, the definition in Eq. (18) is equivalent to the parity of $(C_+^0 - C_+^\pi)$. This is similar in spirit to the "strong $\mathbb{Z}_2$ invariant" that has been invoked to distinguish strong vs. weak (trivial) TI phases[40].

The topological phase diagrams for $\mu = 0$ and $\mu = -1$ are shown in the two bottom panels of Fig. 2, where an odd (even) value of C_+ corresponds to non-trivial (trivial) topological phases, respectively. Notice that although we use, as in 2D, a $\mathbb{Z}$ number to map out the 3D phase diagrams, *the parity* P_C (hence a $\mathbb{Z}_2$ invariant) *suffices to identify all the phases*, since all the QPT lines now separate phases with different parity, unlike in 2D.

Similarly, we may fix $k_y = k_{y,c}, k_z = k_{z,c}$, and define the partial Berry phase sum parity as:

$$P_B = (-1)^{\mathrm{mod}_{2\pi}(B_+)/\pi}, \; B_+ \equiv \sum_{k_y,k_z=0,\pi} (B_{k_y,k_z,1} + B_{k_y,k_z,2}).$$

We find that the resulting values of P_B are consistent with both P_C and P_F throughout the phase diagram. We also recall that in Ref. 43 a many-body generalization of the one-body Berry phase was constructed in the presence of interaction, by properly defining twisted boundary conditions. Thus, an interesting possibility for further exploration is whether the partial Berry phase sum defined here might still characterize the *topological response of an interacting system* with TR and inversion symmetries, provided that only one representative from each TR-pair is selected.

In summary, we may conclude that the parity of the partial Berry phase sum, of the partial Chern sum, and of the partial fermion number are all equivalent to one another: $P_C = P_B = P_F$. Thus, any of them can be used to characterize the $\mathbb{Z}_2$ invariance in our TR-invariant system irrespective of dimensionality, with odd (even) parity corresponding to non-trivial (trivial) topological phases, respectively. That being said, if there are QPT lines between phases that share the same parity (such as in the 2D phase diagram), then a $\mathbb{Z}$ invariant (the partial Chern sum), is needed to distinguish and label all the phases.

B. Bulk-boundary correspondence

As mentioned, a bulk-boundary correspondence generally refers to the relationship between bulk properties of the system in a given phase and the existence and robustness of the corresponding edge states. Specifically, for our TR-invariant Hamiltonian, we formulate the bulk-boundary correspondence in terms of the relation between the bulk $\mathbb{Z}_2$ topological invariants and the *parity*

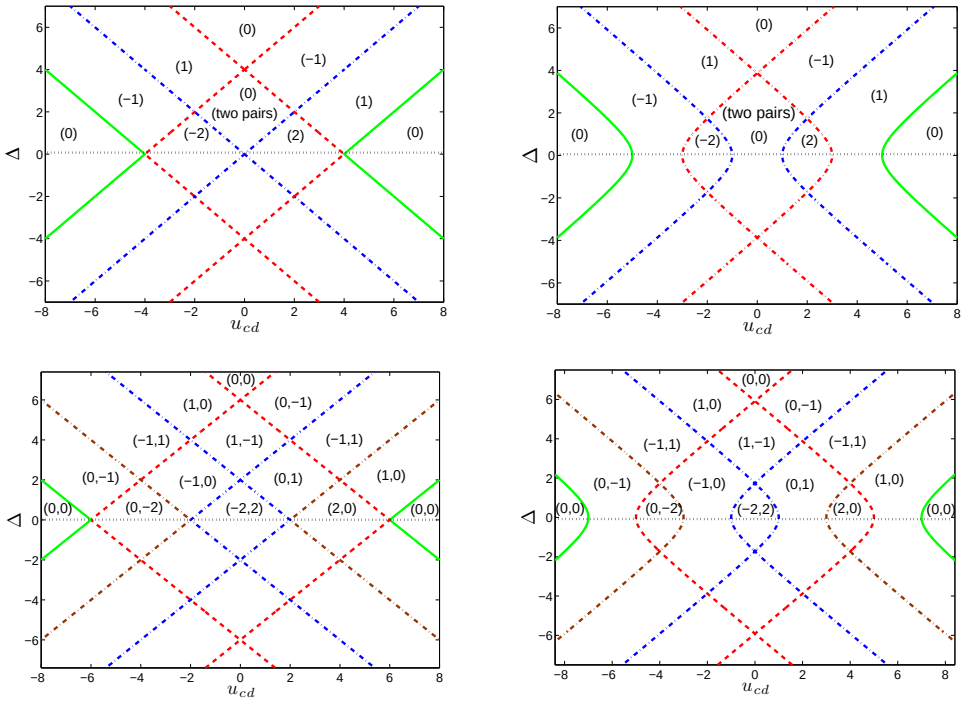

FIG. 2: (Color online) Phase diagrams of the Hamiltonian H_D in 2D [top panels, $\mu = 0$ and $\mu = -1$, respectively] and 3D [bottom panels, $\mu = 0$ and $\mu = -1$, respectively] as a function of u_{cd} and Δ. The topological response is characterized in terms of the partial CN sum C_+ in 2D, and in terms of the partial CN sum of the modes $k_z = k_{z,c}$ (C_+^0, C_+^π) in 3D, the respective values being given in parentheses. The corresponding $\mathbb{Z}_2$ invariant is the parity of the partial CN sum, Eq. (18). System size: $N_x = N_y = N_z = 100$.

of the number of TR-pairs of boundary modes[38]. That is, a bulk phase characterized by odd (even) P_C (or, equivalently, P_B, P_F) is expected to correspond to an odd (even) number of TR-*pairs* of edge states *per boundary*, which are robust against perturbations that preserve the symmetry class of the system (DIII in our case). One should, however, notice that there is no *a priori* reason to expect that the topological numbers that characterize the phases in the bulk phase diagram should be the same that also characterize the bulk-boundary correspondence.

In order to characterize the bulk-boundary correspondence in our model Hamiltonian, we investigate H_D with open boundary conditions (OBC) along one spatial direction, while keeping PBC along the remaining direction(s). Our numerical results indicate that the bulk property $P_C(P_B) = -1(1)$ does correspond to an odd (even) number of *Kramers' pairs of helical edge modes on each boundary*. Since our Hamiltonian exhibits PH symmetry, the quasi-particle annihilation operator $\gamma_{\epsilon_{n,\mathbf{k}}}$ for eigenvalue $\epsilon_{n,\mathbf{k}}$ obeys $\gamma^\dagger_{\epsilon_{n,\mathbf{k}}} = \gamma_{-\epsilon_{n,\mathbf{k}}}$, which identifies such zero-energy modes as Majorana fermions, $\gamma_0^\dagger = \gamma_0$.

The situation is simplest for the 1D system: for instance, when $u_{cd} = 2$, $\Delta = 2$ ($P_B = -1$ in the phase diagram of Fig. 1), one pair of Majorana edge modes exists at each end, while when $u_{cd} = 6$, $\Delta = 2$ ($P_B = 1$ in the phase diagram of Fig. 1), no edge mode is found. Direct calculation also shows that a topologically trivial phase ($P_B = 1$ with $u_{cd} = 0$, $\Delta = 1$ in Fig. 1) can likewise support two pairs of Majorana modes per edge, corresponding to $k_x = 0, k_x = \pi$, respectively. Since the bulk-boundary correspondence for the 2D case has already been extensively discussed in Ref. 30, we focus next on addressing in detail the 3D cubic geometry.

In 3D, we maintain PBC along the x and z directions, and use instead OBC along the y direction (sometimes referring to the resulting 2D boundaries as the right(left) edge). Thus, we can obtain the excitation spectrum $\epsilon_{n,k_x,k_{z,c}}$, by applying a Fourier transformation in the x and z directions. For simplicity, let us focus on the case $\mu = 0$. Since the Dirac cones exist at the TR-invariant modes, we may fix additionally $k_z = k_{z,c} \in \{0, \pi\}$. The resulting excitation spectrum is depicted in Fig. 3 for representative parameter choices. Specifically, panel (a) and (b) correspond to phases that support a total *odd* number of Dirac cones on each edge, that is, two Dirac cones (at $k_x = 0$ and $k_x = \pi$) for $k_z = 0$ and one Dirac cone (at $k_x = 0$) for $k_z = \pi$. This is consistent with the partial Chern sum $C_+^0 = 0$ for $k_z = 0$ and $C_+^\pi = 1$ for $k_z = \pi$, hence [Eq. (18)] $P_C = -1$. Panel (c) and (d) correspond instead to phases supporting a total *even* number of Dirac cones, that is, two Dirac cones at $k_x = 0$ for $k_z = 0$, with two corresponding Kramers' pairs of Majorana modes on each boundary, and no Dirac cone for $k_z = \pi$. This is consistent with the partial Chern sum

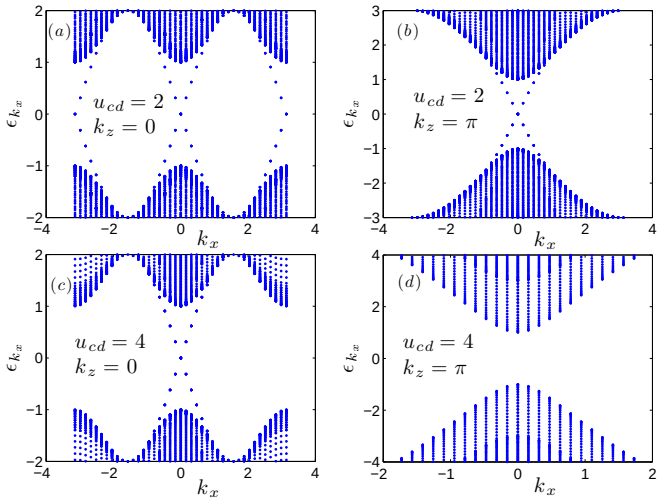

FIG. 3: (Color online) Excitation spectrum of the 3D Hamiltonian H_D with OBC along the y direction, for $\mu = 0, t = 1, \lambda = 1 = \Delta$. Top panels: $u_{cd} = 2$, with $C_+^0 = 0$ for $k_z = 0$ in panel (a), and $C_+^\pi = 1$ for $k_z = \pi$ in panel (b). Bottom panels: $u_{cd} = 4$, with $C_+^0 = 2$ for $k_z = 0$ in panel (c), and $C_+^\pi = 0$ for $k_z = \pi$ in panel (d). Note that the bulk gap scales as $\min(\lambda, \Delta)$, indicating that the edge modes are more stable for stronger SO and superconductivity. System size: $(N_x, N_y, N_z) = (40, 100, 40)$.

$C_+^0 = 2$ for $k_z = 0$ and $C_+^\pi = 0$ for $k_z = \pi$. Similar to both the 1D and 2D cases, an even value of, say, C_+^0 may correspond to a pair of Dirac cones [as in (a)] or it may indicate the absence of Dirac cones altogether [as in (d)].

While gapless Majorana modes in non-trivial TS phases ($P_C = -1$) are protected against boundary perturbations that respect TR and PH symmetry (thus do not change the symmetry class), it is interesting to explicitly verify what happens if $P_C = 1$. Consider, in particular, the situation we discussed above with $C_+ = 2$ [panel (c) in Fig. 3], in which case two Kramers' pairs of helical Majorana modes, say, $(\gamma_1^{(i)}, \gamma_2^{(i)})$, with $\gamma_2^{(i)} = \mathcal{T}\gamma_1^{(i)}\mathcal{T}^{-1}$, $i = 1, 2$, exist at $k_x = 0, k_z = 0$. Suppose that we can express the two co-propagating modes $\gamma_1^{(1)}$ and $\gamma_1^{(2)}$ from each Kramers' pair on a given edge as follows:

$$\begin{cases} \gamma_1^{(1)} = \sum_{j_y=1}^{N_y} (\alpha_{j_y}^{(1)} a_{j_y,\uparrow}^\dagger + \beta_{j_y}^{(1)} b_{j_y,\downarrow}^\dagger + \text{H.c.}), \\ \gamma_1^{(2)} = \sum_{j_y=1}^{N_y} i(\alpha_{j_y}^{(2)} a_{j_y,\uparrow}^\dagger + \beta_{j_y}^{(2)} b_{j_y,\downarrow}^\dagger - \text{H.c.}), \end{cases} \quad (19)$$

for real coefficients $\alpha_{j_y}^{(i)}, \beta_{j_y}^{(i)}$, where we have used the canonical fermion operators defined in Eq. (7) along with $\gamma_1^{(i)\dagger} = \gamma_1^{(i)}$, $i = 1, 2$. Then consider, for example, the following perturbation that acts on the boundary, and preserves TR and PH symmetry, as well as inversion (see also Appendix A for further discussion):

$$H_p = \sum_{k_x, j_y, k_z, \sigma} u_p^{(j_y)} (c_{k_x,j_y,k_z,\sigma}^\dagger c_{-k_x,j_y,-k_z,\sigma} + d_{k_x,j_y,k_z,\sigma}^\dagger d_{-k_x,j_y,-k_z,\sigma}) + \text{H.c.}, \quad (20)$$

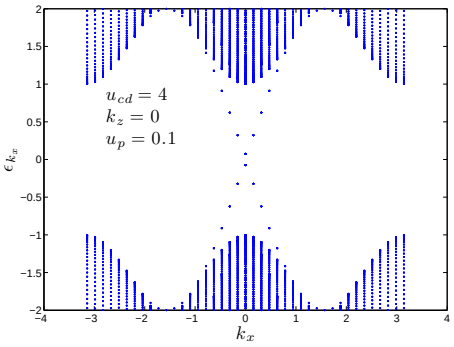

FIG. 4: (Color online) Excitation spectrum of the 3D Hamiltonian H_D with OBC in the y direction and in the presence of the boundary perturbation H_p given in Eq. (20). The relevant parameters are: $\mu = 0, t = 1 = \lambda = \Delta$, and $u_{cd} = 4$, with perturbation strength $u_p = 0.1$. The gapless surface modes clearly become gapped under H_p. System size: $(N_x, N_y, N_z) = (40, 100, 40)$.

where $u_p^{(j_y)} \equiv u_p \neq 0$ for $j_y = 1$ or N_y, and $u_p^{(j_y)} = 0$ otherwise. By invoking degenerate perturbation theory, we can infer that the degeneracy of the zero-energy surface modes is lifted, since explicit calculation yields

$$\langle \Psi_{\mathsf{gs}} | \gamma_1^{(2)\dagger} H_p \gamma_1^{(1)} | \Psi_{\mathsf{gs}} \rangle \neq 0,$$

where $|\Psi_{\mathsf{gs}}\rangle$ is the many-body ground state. The exact excitation spectrum in the presence of H_p is shown in Fig. 4 for $k_z = 0$.

This explicitly illustrates how the presence of an even number of pairs of Majorana modes, such as in the $C_+ = 2$ phase in 3D, makes such modes generally non-robust against boundary perturbations, even if the symmetry class of the system is unchanged. Therefore, a distinctive property of a 3D TR-invariant TS is the presence of an *odd* number of Dirac cones, corresponding to an *odd* number of pairs of helical Majorana surface modes, similar to the 1D and 2D cases. While this might seem to conflict with the robust behavior predicted from the topological classification[49] for the DIII class in 3D, this apparent contradiction can be resolved by noting that such a classification strictly must be applied within "irreducible" blocks where *only* generic symmetries such as TR and PH are satisfied. While care is needed in interpreting the free-fermion topological classification in the presence of inversion symmetry [see Appendix C in Ref. 49] and, more generally, interaction effects[51], our model additionally exhibits "hidden" discrete symmetries which, although hard to identify *a priori*, should be taken into account in principle. For instance, we have explicitly verified that one such $\mathbb{Z}_2 \otimes \mathbb{Z}_2 \otimes \mathbb{Z}_2 \otimes \mathbb{Z}_2$ hidden symmetry exists in the limit $\mu = 0$, $\lambda = t$, and is broken by the above perturbation H_p (see Appendix A).

In summary, topologically non-trivial (trivial) phases with odd (even) P_C (P_B, P_F) corresponds to an odd (even) number of Dirac cones (or points, depending on

dimension). Thus, our model Hamiltonian H_D in Eq. (2) exhibits qualitatively similar behavior regardless of dimensionality, in the sense that both trivial and nontrivial TS phases exist in all cases. Thanks to the richer phase structure, however, more possibilities arise in 3D for different phases to exist. Interestingly, while QPT lines always separate odd-parity TS from even-parity trivial phases, a vanishing gap and thus QPT lines can also occur between regions of the phase diagram sharing similar topological features in 2D.

IV. RESPONSE TO TIME-REVERSAL SYMMETRY BREAKING PERTURBATIONS

Since the Hamiltonian H_D preserves TR symmetry, the gapless nature of the Kramers' pair(s) of helical Majorana modes in a TS phase is protected against perturbations that preserve TR symmetry. It is nevertheless interesting to explore how such robustness properties are modified when TR symmetry is broken in different ways, and the extent to which these changes are reflected in the bulk topological indicators. As a result of explicitly breaking TR symmetry (thus bringing the system to class D, according to Ref. 39), we expect that different topological invariants are needed to characterize the topological phases, as well as a different formulation of the bulk-boundary correspondence. Specifically, as we shall see in what follows, $\mathbb{Z}_2$ topological invariants may now be constructed from the parity of the *full* (rather than partial) Chern or Berry phase sum, with the bulk-boundary correspondence requiring that an odd (even) value of the latter also implies an *odd (even) number of Majorana edge modes (as opposed to Majorana pairs) on each boundary.*

To the best of our knowledge, most investigations aiming to explore the robustness of topological phases under TR-symmetry breaking have involved a TI model as their starting point, see *e.g.* Refs. 53–56. In this section, we shall focus on studying our TS model first in the presence of a uniform (bulk) Zeeman field along different directions, intended as an external control parameter, and then in the presence of different kinds of internal (uncontrollable) magnetic impurities. Next, we will proceed to quantitatively investigate the effect of TR-symmetry breaking by moving away from the limit of exactly π-shifted superconducting gaps [Eq. (6)], and again reconsider the effect of and interplay with an applied Zeeman field. While we shall primarily address a 2D geometry, in the light of our analysis in Sec. III and as it will become clear through the discussion, the main features emerging for the 2D case will remain qualitatively valid with some natural modifications for 1D and 3D as well.

A. Majorana modes under a static magnetic field

Throughout this section, we shall continue to assume that $\Delta_c = -\Delta_d$, and consider a total Hamiltonian of the form $H \equiv H_D + H_M$, where H_D is given in Eq. (2) and

$$H_M = \sum_{\nu=x,y,z} H_M^{(\nu)}, \quad H_M^{(\nu)} = \sum_j h_\nu^{(j)} \psi_j^\dagger \sigma_\nu \psi_j. \qquad (21)$$

Here, $h_\nu^{(j)}$ represents the strength of the magnetic field/impurity along the ν direction at site j, and the sum extends over all lattice sites or over boundary sites only, depending on whether a bulk or boundary field is considered. With reference to the spin (z) quantization axis, we shall refer to the z (x, y) as longitudinal (transverse) directions, respectively.

1. *Effect of a uniform longitudinal magnetic field*

Let us begin by considering the response of the bulk to a uniform z-magnetic field, that is, $h_\nu^{(j)} = h_z \neq 0$. Remarkably, an analytical solution for the full spectrum still exists for PBC by employing the diagonalization procedure described in Sec. II A, thanks to the fact that the SO coupling H_{so} has no component along z (see also Appendix C). That is, the total Hamiltonian can still be rewritten as in Eq. (4), with $\hat{H}'_{\mathbf{k}} = \hat{H}'_{+,\mathbf{k}} \oplus \hat{H}'_{-,\mathbf{k}}$ defined in Eqs. (8)-(9), except that now we replace $m_{\mathbf{k}} \mapsto m_{\pm,\mathbf{k}} = m_{\mathbf{k}} \pm h_z$, in the corresponding expression for $\hat{H}'_{\pm,\mathbf{k}}$. With this substitution, the excitation spectrum $\epsilon_{n,\mathbf{k},+}$ ($\epsilon_{n,\mathbf{k},-}$) obtained from diagonalizing $\hat{H}'_{+,\mathbf{k}}$ ($\hat{H}'_{-,\mathbf{k}}$) is formally still given by Eq. (10). Thus, it is clear that the effect of the longitudinal Zeeman field is to formally replace $u_{cd} \mapsto u_{cd} \pm h_z$ for $\hat{H}'_{\pm,\mathbf{k}}$, respectively. QPTs occur when the excitation gap closes, that is, when either $\epsilon_{2,\mathbf{k},+} = 0$ or $\epsilon_{2,\mathbf{k},-} = 0$ (for general $\Delta \neq 0$), which determines the QPT lines as $m_{\pm,\mathbf{k}_c} = \pm\,\Omega$.

Since TR symmetry is broken, the full sum of the CNs over the two occupied negative bands of *both* $\hat{H}'_{+,\mathbf{k}}$ and $\hat{H}'_{-,\mathbf{k}}$ need no longer be zero. Thus, we can use the parity of this full Chern sum, $\tilde{P}_C$, as a $\mathbb{Z}_2$ invariant. However, in order to make a comparison between *partial* Chern sums with and without magnetic field, we still calculate, following Eq. (15), the partial Chern sums ($C_{+,\pm}$) of the two occupied negative bands of $\hat{H}'_{\pm,\mathbf{k}}$ separately (say, $C_{1,\pm}$ and $C_{2,\pm}$) and construct the parity invariant as follows:

$$\tilde{P}_C \equiv (-1)^{\mathrm{mod}_2(C_{+,+}+C_{+,-})}, \quad C_{+,\pm} \equiv C_{1,\pm} + C_{2,\pm},$$

in such a way that $C_{+,+} = -C_{+,-} = C_+$ [given by Eq. (16)] in the absence of magnetic field.

The resulting topological phase structure is shown in Fig. 5, where the two numbers reported in parentheses are the two partial Chern sums, $C_{+,+}$ and $C_{+,-}$, respectively. Two remarks are in order. First, despite the fact that, as we have verified, *no* singular behavior of the derivatives of the many-body ground-state energy with respect to h_z develops at $h_z = 0$, one should treat the phases along the TR-invariant line $h_z = 0$ as being different from those in the TR-broken region

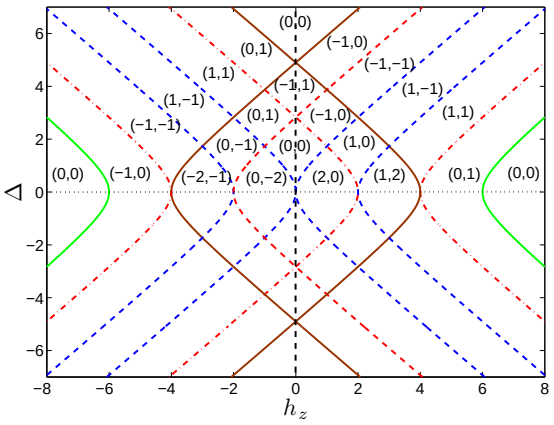

FIG. 5: (Color online) Topological phase diagram of the 2D Hamiltonian $H_D + H_M$, with $H_M \equiv H_M^{(z)}$ being a longitudinal Zeeman field with strength h_z. The remaining parameters are $t = 1$, $u_{cd} = 1$, $\mu = -1$, for arbitrary $\lambda \neq 0$. The topological response is characterized via the partial CN sum $(C_{+,+}, C_{+,-})$ from the occupied bands of $\hat{H}'_{+,\mathbf{k}}$ and $\hat{H}'_{-,\mathbf{k}}$, respectively. The horizontal black dotted-line has the same meaning of the zero-field case. The vertical black dotted-line indicates that a different classification of phases applies along the TR-invariant line $h_z = 0$, see text.

$h_z \neq 0$. This is because the process of adiabatic connection between two regions in parameter space must be carried out *without* changing the basic symmetry class in order for these regions to be meaningfully thought as belonging to one and the same topological phase[49]. Second, in a real physical system, an excessively strong magnetic field can destroy superconductivity. Thus, we have also performed self-consistent calculations, along the lines of Appendix B, in order to have at least some indication on the degree of stability of different phases in Fig. 5. Our numerical results suggest that the required range of Δ remains accessible in the presence of magnetic field for all the phases not too far from the center of the phase diagram, labeled with $(C_{+,+}, C_{+,-}) = (2,0), (0,-2), (0,0), (-1,0), (0,1), (-1,1)$. Specifically, in order to get a rough order-of-magnitude estimate, let us assume a material with narrow bandwidth, say between 10 meV $\sim$ 100 meV, indicating that the tight-binding coupling strength t is in the range 2 meV $\sim$ 20 meV. The value $h_z = 0.1$ may then correspond to a field strength between 0.2 meV $\sim$ 2 meV (2 $\sim$ 20 T, respectively). Since h_z can be arbitrarily close to zero in the above-mentioned phases however, the corresponding magnetic field strengths can safely be below the critical field strength in superconductors.

Similar to the case when TR symmetry is conserved, we may still establish a direct connection between the invariant $\tilde{P}_C$ defined above and the *full* fermion number parity of the TR-invariant modes $\tilde{P}_F$. Following the same procedure outlined in Sec. II B, we find that when $|m_{+,\mathbf{k}_c}| > |\Omega|$, the ground state of each mode $\mathbf{k}_c$ in $\hat{H}'_{+,\mathbf{k}}$ belongs to the sector with odd fermion parity, that is, $P_{+,\mathbf{k}_c} = e^{i\pi(a^\dagger_{\mathbf{k}_c,\uparrow} a_{\mathbf{k}_c,\uparrow} + b^\dagger_{\mathbf{k}_c,\downarrow} b_{\mathbf{k}_c,\downarrow})} = -1$, otherwise it is in the sector with even fermion parity $P_{+,\mathbf{k}_c} = 1$. Similar results for the fermion parity $P_{-,\mathbf{k}_c}$ of the ground state of each mode $\mathbf{k}_c$ in $\hat{H}'_{-,\mathbf{k}}$ are obtained by analyzing the relation between $|m_{-,\mathbf{k}_c}|$ and $|\Omega|$. As a result of breaking TR symmetry, however, $P_{-,\mathbf{k}_c}$ *need not* be equal to $P_{+,\mathbf{k}_c}$, just like $C_{+,-}$ is not necessarily the opposite to $C_{+,+}$. Nonetheless, let us define, in analogy to Eq. (17),

$$\tilde{P}_F \equiv \prod_{\mathbf{k}_c} P_{+,\mathbf{k}_c} P_{-,\mathbf{k}_c}.$$

Then, by analyzing the relation between $|m_{\pm,\mathbf{k}_c}|$ and $|\Delta|$ for each $\mathbf{k}_c$, we can see that the TS (trivial) phases with $\tilde{P}_C = -1(1)$ correspond to the ground state with $\tilde{P}_F = -1(1)$, as anticipated. In contrast to the TR-invariant case, note that it is *necessary* to take into account the CNs or fermion parity of the occupied bands in both $\hat{H}'_{\pm,\mathbf{k}}$, in order for this correspondence to hold.

Let us now focus on exploring the effect of the magnetic field on the Majorana edge states. To do so, as before we study the 2D Hamiltonian $H = H_D + H_M$ on a cylinder (PBC along x, and OBC along y), with the corresponding excitation spectrum, ϵ_{n,k_x}, obtained by applying a Fourier transformation in the x-direction only. In order to demonstrate the bulk-boundary correspondence when TR symmetry is broken, that is, the correspondence between a bulk with $\tilde{P}_C = 1(-1)$ and the presence of an even (odd) number of Majorana edge modes, we show in Fig. 6 two representative cases with $\tilde{P}_C = 1(-1)$ respectively. Specifically, for even $\tilde{P}_C$ [top panel, $C_{+,+} = 1, C_{+,-} = -1$], two helical Majorana edge states exist on each boundary, whereas for odd $\tilde{P}_C$ [bottom panel, $C_{+,+} = 0, C_{+,-} = -1$], only one chiral Majorana edge state on each boundary, which is consistent with the above bulk-boundary correspondence. Accordingly, the top (bottom) panel of Fig. 6 corresponds to a trivial (non-trivial) topological phase.

Interestingly, if the magnetic field is turned off while keeping all the other control parameters unchanged in the trivial phase corresponding to the top panel, the same partial Chern sums $C_{+,+} = 1, C_{+,-} = -1$ still hold in the limit $h_z \to 0$. These values, however, correspond now to a *non*-trivial TR-invariant TS since the $\mathbb{Z}_2$ invariant is characterized by the (odd) parity of the *partial* Chern sum when TR symmetry is preserved, rather than the parity of the Chern sum for *all* the occupied bands. This illustrates how the same topological number may in fact correspond to completely different phases. The key point here is that *the topological invariant changes when the basic symmetry class changes*, as a consequence of TR symmetry being broken. Although, as already remarked, no singular behavior develops at $h_z = 0$, a topological QPT still takes place in this sense, solely signaled by the change of the underlying topological invariant.

The observation that the two situations for $h_z = 0$ and $h_z \neq 0$ in the above discussion correspond to non-trivial and trivial topological phases, respectively, may be

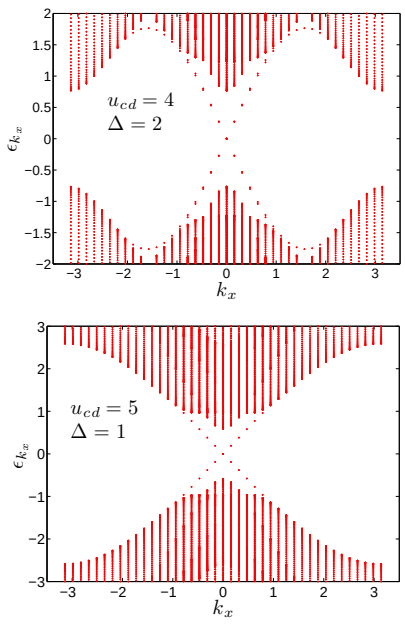

FIG. 6: (Color online) Excitation spectrum of the 2D Hamiltonian $H_D + H_M$ on a cylinder, with $H_M = H_M^{(z)}$ being a longitudinal Zeeman field with strength $h_z = 1$, and $\mu = -1, t = 1 = \lambda$. Top panel: $u_{cd} = 4, \Delta = 2$, $\tilde{P}_C = 1$. Two (helical) Majorana edge states exist on each boundary, corresponding to a trivial phase. Bottom panel: $u_{cd} = 5, \Delta = 1$, $\tilde{P}_C = -1$. One (chiral) Majorana edge state exist on each boundary, corresponding to a TS phase. System size: $(N_x, N_y) = (40, 100)$.

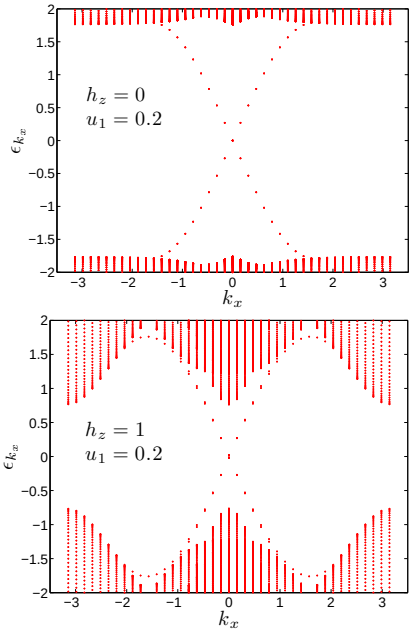

FIG. 7: (Color online) Excitation spectrum of the 2D Hamiltonian $H_D + H_M + H_b$ on a cylinder, with $H_M = H_M^{(z)}$ being a longitudinal Zeeman field with strength h_z and H_b a backscattering potential with strength $u_1 = 0.2$ respectively, for $\mu = -1, t = 1 = \lambda, u_{cd} = 4, \Delta = 2$. Top panel: TR-invariant case, $h_z = 0$. The two Majorana modes on each edge form a Kramers' pair and remain gapless under H_b. Bottom panel: TR-broken case, $h_z = 1$. The two Majorana modes on each edge form a quasi-TR pair, note the appearence of a gap in the edge spectrum. System size: $(N_x, N_y) = (40, 100)$.

explicitly confirmed by investigating the response of the gapless edge states under the effect of a TR-preserving back-scattering interaction. For instance, let us consider the following boundary perturbation:

$$H_b = i \sum_{k_x, j_y} u_1^{(j_y)} (c^\dagger_{k_x, j_y, \uparrow} d_{k_x, j_y, \uparrow} - c^\dagger_{k_x, j_y, \downarrow} d_{k_x, j_y, \downarrow}) + \text{H.}c.,$$

where $u_1^{(j_y)} = u_1 \neq 0$ for $j_y = 1$ or $j_y = N_y$, and $u_1^{(j_y)} = 0$ otherwise. Let us also introduce the terminology of a "quasi-TR-pair" to refer to two gapless Majorana edge modes when (i) TR symmetry is broken, yet, (ii) the relationship $C_{+,+} = -C_{+,-}$ still holds for the corresponding bulk. A comparison between the robustness of a Kramers' pair and a quasi-TR-pair of Majorana modes against H_b is shown in Fig. 7. As one can see, the Kramers' pairs of Majorana modes are robust (top panel), whereas the quasi-TR pairs are not, in the sense that they become gapped, with a gap scaling linearly in u_1 (bottom panel). Thus, gapless TR-pairs of edge modes of the zero-field Hamiltonian H_D *may remain gapless in the presence of a magnetic field. However, their degree of robustness against subsequent TR-preserving perturbations is, in general, different* as compared to the original Kramers' pairs. It is worth noting that a similar behavior was also reported recently in the context of a TR-invariant quantum spin Hall system[53], where a pair of gapless edge states was found to remain gapless when an external magnetic field was added. These gapless edge states would however become gapped in the presence of backscattering, indicating a low-dissipation (but not dissipation-less) spin transport.

Unlike in other models where a Zeeman magnetic field is required for the very existence of Majorana modes (see, for instance, in Refs. 50,57), we iterate that this is clearly *not* the case in our multi-band system. Rather, the Zeeman field may be viewed as a control knob for potentially tuning the emergence/disappearance of Majorana modes. For instance, with reference to the phase diagram in Fig. 5, imagine that for a fixed value of Δ, say $\Delta = 3.2$, the magnetic field h_z is increased from $h_z = 0$ to $h_z = 8$. Then it turns out that the number of Majorana edge modes changes in the following way: 2 (one TR-pair, as $h_z = 0$) $\to$ 2 (one quasi-TR-pair)$\to$ 3 $\to$ 2 $\to$ 1, which effectively turns the original strong TS into a weak/trivial one depending on the applied field strength. Likewise, if Δ is instead fixed at, say, $\Delta = 1$, a non-zero h_z can turn a weak TS into to a non-trivial topological phase with only one robust Majorana edge mode on each boundary. The usefulness of a Zeeman field as a tuning mechanism in the presence of an additional TR-breaking perturbation will also be further discussed in Sec. IV B.

2. *Effect of uniform transverse magnetic fields*

Let us now briefly consider the case where a Zeeman field is instead applied in a transverse (x or y) direction, with focus on the changes induced in the edge spectrum. Specifically, imagine first that the magnetic field acts along x, that is, $h_\nu^{(j)} = h_x$ in Eq. (21). In the presence of such a field, the total Hamiltonian $H_D + H_M$ on a cylinder can no longer be decoupled into two $4N_y \times 4N_y$ matrices for each momentum mode k_x (see Appendix C). We can nevertheless obtain physical insight by examining specific cases. Imagine, in particular, that the system is in a TS phase when $h_x = 0$, say corresponding to $\mu = -1$, $u_{cd} = 4, \Delta = 1$, with reference to the phase diagram in Fig. 2 [top right panel], and imagine that we still express the energy eigenvectors in the basis of canonical fermion annihilation operators a_σ and b_σ defined in Eq. (7) when $h_x = 0$. Then we may represent the two TR-invariant Majorana edge modes (γ_1, γ_2), $\gamma_2 = \mathcal{T}\gamma_1\mathcal{T}^{-1}$, that exist for $k_x = 0$ on each boundary in the form

$$\begin{cases} \gamma_1 = \sum_{j_y=1}^{N_y} (\alpha_{j_y} a^\dagger_{j_y,\uparrow} + \beta_{j_y} b^\dagger_{j_y,\downarrow} + \text{H.c.}), \\ \gamma_2 = \sum_{j_y=1}^{N_y} (\alpha_{j_y} a^\dagger_{j_y,\downarrow} - \beta_{j_y} b^\dagger_{j_y,\uparrow} + \text{H.c.}), \end{cases} \tag{22}$$

for suitable real coefficients [cf. Eq. (19)]. Direct calculation shows that the matrix element with respect to the many-body ground state vanishes:

$$\langle \Psi_{\text{gs}} | \gamma_2^\dagger H_M^{(x)} \gamma_1 | \Psi_{\text{gs}} \rangle = 0. \tag{23}$$

Similarly, one also finds that:

$$\langle \Psi_{\text{gs}} | \gamma_2^\dagger H_M^{(y)} \gamma_1 | \Psi_{\text{gs}} \rangle \neq 0. \tag{24}$$

Thus, according to degenerate perturbation theory, a field in the x direction cannot lift the degeneracy of the gapless Majorana edge modes supported by H_D, whereas in general a field along the y direction does. These conclusions have been confirmed by explicit numerical calculation, with illustrative results shown in Fig. 8.

It is worth noting that the different roles that magnetic fields in the x vs. y direction play in our model is ultimately a consequence of the different boundary conditions imposed in these directions, PBC (OBC) along x (y) directions, respectively. Should the latter be interchanged, then the effect of transverse perturbations along x and y would be as well. Furthermore, even if the edge spectrum remains gapless under $h_x \neq 0$, the edge modes no longer form Kramers' pairs. Thus, similarly to the behavior found in the presence of a z-field [Fig. 7], these modes are not expected in general to have the same degree of robustness against disorder/backscattering as they have in the TR-invariant case.

As a side remark, it is also interesting to observe that in the limit $\Delta \to 0, \mu \to 0$, where the model Hamiltonian H_D describes a TI, a perturbation in the x-direction does *not* lift the degeneracy of the gapless edge modes either, despite the lack of Majorana fermions. As a result of PH

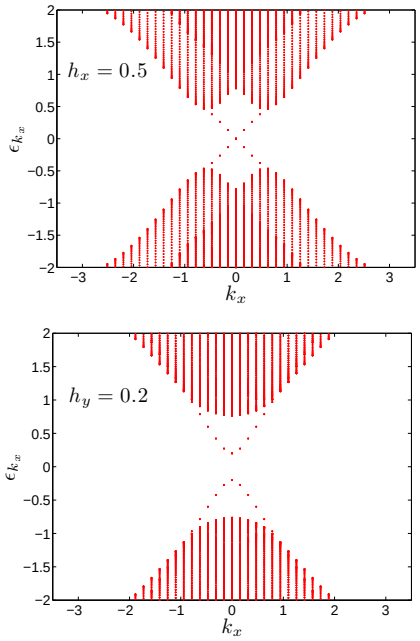

FIG. 8: (Color online) Excitation spectrum of the 2D Hamiltonian $H_D + H_M$ on a cylinder, with $H_M = H_M^{(\nu)}$ being a uniform transverse field, for $\mu = -1, t = 1 = \lambda, u_{cd} = 4, \Delta = 1$. Top panel: x-field, with strength $h_x = 0.5$. The edge spectrum remains gapless. Bottom panel: y-field, with strength $h_y = 0.2$. The edge spectrum becomes gapped. System size: $(N_x, N_y) = (40, 100)$.

symmetry, the two fermionic TR-invariant edge modes at the Dirac point can now be written as ($h_x = 0$):

$$\begin{cases} \gamma_1 = \sum_{j_y=1}^{N_y} \alpha_{j_y} (a_{j_y,\uparrow} + b_{j_y,\downarrow}), \\ \gamma_2 = \sum_{j_y=1}^{N_y} \alpha_{j_y} (a_{j_y,\downarrow} - b_{j_y,\uparrow}), \end{cases}$$

that is, the quasi-particles $a_{j_y,\uparrow}(a_{j_y,\downarrow})$ and $b_{j_y,\downarrow}(b_{j_y,\uparrow})$ behave as if they were particle-hole pairs. The possibility that edge states in a TI may remain robust despite TR-breaking was recently noted in a different context[56].

3. *Effect of magnetic impurities*

In reality, even in the absence of external perturbations, magnetic fields are inevitably present due to various kinds of impurities in the material. Thus, it is important to get a sense of what effect such magnetic fields will have on Majorana modes, a main difference with respect to the uniform-field case being that translational symmetry is now explicitly broken along one or more spatial directions. While more complex scenarios can be envisioned, we limit ourselves here to impurity fields acting along a single direction. In particular, we consider a longitudinal (z) impurity field in a 2D geometry, and still assume PBC (OBC) in the x (y) direction, respectively.

Suppose that the system is in a TS phase, with a pair of Majorana edge states on each boundary. Two scenarios

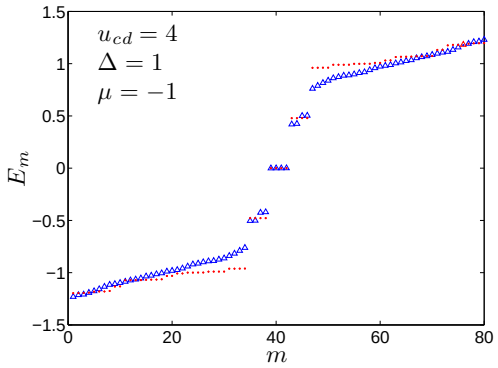

FIG. 9: (Color online) Single-particle excitation spectrum of the 2D Hamiltonian $H_D + H_M$ on a cylinder, with $H_M = H_M^{(z)}$ representing a longitudinal impurity magnetic field, for $\mu = -1, t = 1 = \lambda, u_{cd} = 4, \Delta = 2$. The blue triangle correspond to case (i), with a single magnetic impurity with strength $h_z = 0.5$ on each boundary, whereas the red dots correspond to uniformly distributed random magnetic impurities on each boundary (averaged over 10 different realizations). System size: $(N_x, N_y) = (16, 16)$.

may be physically interesting:

(i) a *single* magnetic impurity on each boundary, in which case we may let, for instance, $h_\nu^{(j)} = h_z \neq 0$, for $j \in \{(1,1), (N_x, N_y)\}$, and $h_\nu^{(j)} = 0$ otherwise in Eq. (21);

(ii) *random* magnetic impurities on each boundary, in which case we may let, for instance, $h_z^{(j)}$ in Eq. (21) to be uniformly distributed random numbers in $[0, 1]$.

As a result of explicitly breaking translational symmetry, the total Hamiltonian is now be written directly in real space in the form

$$H_D + H_M = \sum_{i,j} \left(\psi_i^\dagger, \psi_i^T\right) \hat{H}_{i,j} \begin{pmatrix} \psi_j \\ (\psi_j^\dagger)^T \end{pmatrix},$$

for a suitable matrix $\hat{H}_{i,j}$. Numerical results obtained by diagonalizing $H_D + H_M$ in the single-particle sector $\hat{H}_{i,j}$ in the two cases are shown in Fig. 9, where the label E_m corresponds to the mth single-particle eigenvalue and only the energy eigenvalues near zero are displayed. Despite TR symmetry being broken, gapless edge modes may still be inferred to persist in both cases in the thermodynamic limit: in case (i), the minimum gap in the edge spectrum is about 10^{-8} (10^{-12}) for system size 16×16 (24×24), and similarly in case (ii) such a minimum gap is 10^{-8} (10^{-11}) for system size 16×16 (24×24), respectively. Hence, the Majorana edge modes are stable against the effect of either single or random boundary perturbation along the z direction.

Since, from our analysis for a uniform field [Eqs. (23)-(24)], we know that the edge spectrum of our Hamiltonian remains gapless under h_x perturbations, we may additionally conclude that Majorana modes remain gapless in the presence of magnetic impurities (single or random) along x, whereas magnetic impurities along the y direction will generally result in gapped edge modes.

Although, as anticipated, we have focused above on the 2D case, a similar approach may be employed to determine the magnetic-field response for the 1D and 3D models. The situation is straightforward in 1D: the exact phase diagram under a z-field can be determined as in Sec. IV A 1 and, if either z or y impurity fields are present, edge modes remain gapless – unlike for a x-field due to the OBC imposed along x. In 3D, although z is no longer a special direction for the zero-field Hamiltonian, we may still obtain the exact phase diagram under a longitudinal magnetic field if we fix $k_z = k_{z,c}$ as we also did in Sec. II A. If we still impose OBC along y, then similar to the 2D case, gapless edge modes remain gapless for magnetic fields along the x or z directions, whereas they become gapped for a field along y.

B. Majorana modes away from π-shifted gaps

Throughout our discussion so far, we have assumed that the superconducting pairing gaps are exactly π-shifted, $\Delta_c = -\Delta_d$. Both because this condition need not be (exactly) satisfied in practice, and in order to gain additional insight on the role it plays, it is interesting to ask what happens if it is relaxed, while still treating the gaps as tunable parameters. For simplicity, let us examine separately the two main mechanisms by which the equality $\Delta_c = -\Delta_d$ may break:

(i) the two gaps may be mismatched in *amplitude*, that is, $|\Delta_c| \neq |\Delta_d|$ but the corresponding phases still obey $\theta_c - \theta_d = \pi$;

(ii) the two gaps may be mismatched in *phase*, that is, $|\Delta_c| = |\Delta_d|$ but $\theta_c - \theta_d \neq \pi$, say, $\theta_c - \theta_d = \pi + \epsilon$.

While TR symmetry is respected in case (i), this is no longer the case unless $\epsilon = m\pi$, $m \in \mathbb{Z}$, in case (ii). Representative numerical results illustrating the effect of these two perturbations in 2D are shown in Fig. 10, where the value Δ_{edge} is twice the energy difference between the edge and zero energy states. As the data clearly show, Majorana edge states remain stable (gapless) against an amplitude mismatch as in (i) (see also Ref. 32), whereas

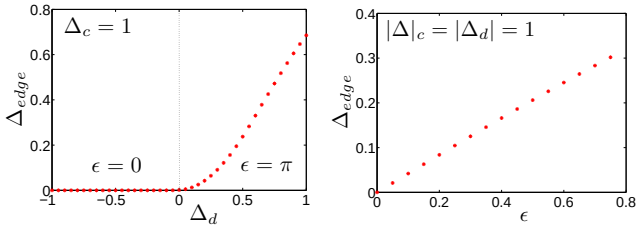

FIG. 10: (Color online) Minimum gap Δ_{edge} of the edge spectrum of the 2D Hamiltonian H_D on a cylinder, away from the symmetry point $\Delta_c = -\Delta_d$. Top panel: effect of a TR-preserving amplitude mismatch in the absence ($\epsilon = 0$) or in the presence ($\epsilon = \pi$) of a concomitant phase mismatch. Bottom panel: effect of a TR-breaking phase mismatch perturbation. System size: $(N_x, N_y) = (40, 100)$.

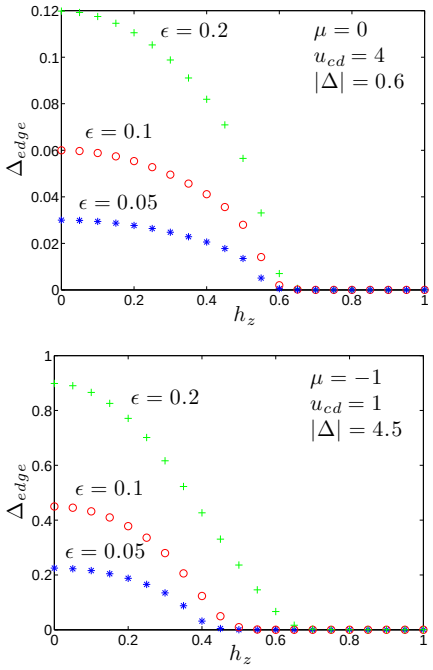

FIG. 11: (Color online) Effect of a longitudinal Zeeman field in restoring gapless Majorana excitations in the presence of a phase mismatch $\epsilon \neq 0$, for two different sets of parameters in 2D. In the bottom panel, the minimum magnetic-field strength required for restoring gapless Majorana modes depends more strongly upon ϵ as a result of the relatively large amplitude of $|\Delta|$. System size: $(N_x, N_y) = (40, 100)$.

they become gapped for a phase mismatch as in (ii), with a minimum gap that scales linearly with ϵ.

Interestingly, it is possible to counter the effect of a non-zero ϵ by applying a Zeeman longitudinal field in the bulk. In particular, recalling the analysis of Sec. IV A 1, we find that in order to restore gapless Majorana excitations, it is necessary to have a sufficiently strong magnetic field to allow the *unperturbed* Hamiltonians $\hat{H}'_{+,k}$ (with $u'_{cd} \equiv u_{cd} + h_z$) and $\hat{H}'_{-,k}$ (with $u'_{cd} \equiv u_{cd} - h_z$) to belong to different phases in the corresponding phase diagram (Fig. 2). Explicit numerical results are shown in Fig. 11: in the top panel, the original Hamiltonian with $\epsilon = 0, h_z = 0$ is in the TR-invariant TS phase with CNs $C_{+,+} = 1, C_{+,-} = -1$, supporting a TR Kramers' pair of Majorana modes on each edge. If $\epsilon \neq 0$ and the Zeeman field strength is sufficiently large, $h_z \gtrsim 0.6$, the CNs become $C_{+,+} = 0, C_{+,-} = -2$, and the edge states become correspondingly gapless, with two *chiral* (co-propagating) Majorana modes on each boundary (note that the latter do *not* form a quasi-TR-pair according to our definition). Similarly, in the bottom panel, the original Hamiltonian with $\epsilon = 0, h_z = 0$ is in the TR-invariant TS phase with CNs $C_{+,+} = -1, C_{+,-} = 1$. If, again, the Zeeman field strength is sufficiently large, the CNs become $C_{+,+} = -1, C_{+,-} = 0$, and gapless Majorana excitations are restored. In fact, since one of the original Majorana modes fuses with the bulk and thus only *one* edge mode exists on each boundary, this mode retains robustness against the effect of TR-preserving backscattering perturbation, despite TR being explicitly broken.

In order to verify the physical relevance of using relatively strong magnetic fields to restore Majorana excitations, we have again also performed self-consistent calculations of the superconducting order parameter Δ for representative situations, in particular for the situation just discussed, corresponding to the bottom panel of Fig. 11. Our results show that values of the pairing gap $|\Delta|$ in the given range can still be achieved self-consistently even in the presence of the required magnetic field. Lower magnetic-field strengths can also in principle be obtained by suitably modifying the parameter u_{cd}.

Mathematically, the fact that a magnetic field can restore gapless Majorana excitations may be understood through degenerate perturbation theory. Suppose that $h_z = 0$ and $\epsilon = 0$, the TR-pair of Majorana edge modes $(\gamma_{1,2})$ in the phase with $C_{+,+} = -C_{+,-} = 1$ may be expressed as Eq. (22). Now let $\Delta_d = -\Delta_c e^{i\epsilon} = -\Delta_c - i\epsilon\Delta_c + O(\epsilon^2)$. Then direct calculation shows that the effect of the perturbing term in H_D scales as

$$\langle \Psi_{\mathbf{gs}} | \gamma_2^\dagger \Big(-i\epsilon\Delta_c \sum_j d^\dagger_{j,\uparrow} d^\dagger_{j,\downarrow} + \text{H.c.} \Big) \gamma_1 | \Psi_{\mathbf{gs}} \rangle \sim \epsilon, \quad (25)$$

consistent with the behavior reported in Fig. 10. When a weak magnetic field is applied in the above case, the TR-pair of Majorana edge modes become quasi-TR-pair (since $C_{+,+} = -C_{+,-} = 1$ remains true), and maybe expressed in the form

$$\begin{cases} \tilde{\gamma}_1 = \sum_{j_y=1}^{N_y} \left(\tilde{\alpha}_{j_y} a^\dagger_{j_y,\uparrow} + \tilde{\beta}_{j_y} b^\dagger_{j_y,\downarrow} + \text{H.c.} \right), \\ \tilde{\gamma}_2 = \sum_{j_y=1}^{N_y} \left(\tilde{\alpha}'_{j_y} a^\dagger_{j_y,\downarrow} - \tilde{\beta}'_{j_y} b^\dagger_{j_y,\uparrow} + \text{H.c.} \right), \end{cases} \quad (26)$$

for real expansion coefficients. [Notice that, in comparison to Eq. (22) for a TR-pair of Majorana modes, the form of Eq. (26) is still the same, but the coefficients $\tilde{\alpha}'_{j_y}(\tilde{\beta}'_{j_y})$ are in general different from $\tilde{\alpha}_{j_y}(\tilde{\beta}_{j_y})$.] One may then show that Eq. (25) remains valid with $\gamma_{1,2}$ replaced by $\tilde{\gamma}_{1,2}$, leaving the edge spectrum gapped, as seen in Fig. 11. On the other hand, if $\epsilon = 0$ and $h_z \neq 0$ is large, as in the above case where $C_{+,+} = 0, C_{+,-} = -2$, the two chiral Majorana edge modes on one boundary can no longer be regarded as a quasi-TR pair but should rather be expressed as in Eq. (19). By introducing now the effect of the phase-mismatch perturbing term as done above $(-i\epsilon\Delta_c)$, a similar calculation shows that the degeneracy between the two Majorana modes cannot be lifted, despite the fact that they are *not* a quasi-TR pair.

This is interesting as it demonstrates that *"unpaired" Majorana modes need not be, a priori, less robust than modes forming a (quasi-)TR pair*: A TR Majorana pair is guaranteed to behave robustly against perturbations that preserve TR symmetry, however, once the latter is broken (via h_z in our example), it may happen that unpaired Majorana modes are more robust against additional TR-breaking (such as a phase mismatch, and possibly even

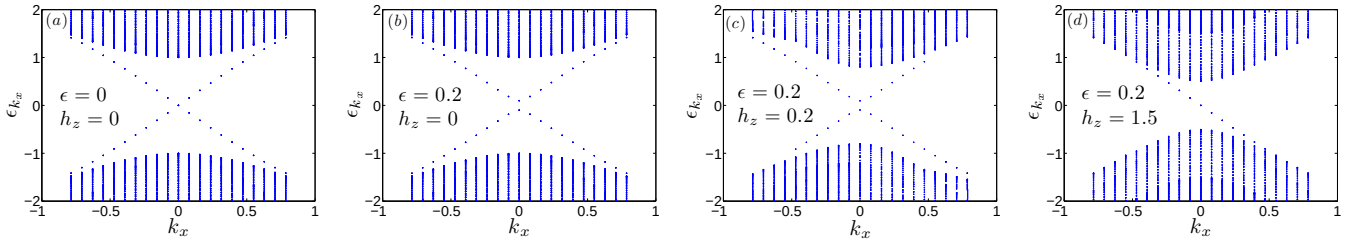

FIG. 12: (Color online) Excitation spectrum for the 2D Hamiltonian $H_D + H_M^{(z)}$ on the cylinder, for $\mu = 0$, $u_{cd} = 4$, $|\Delta_c| = |\Delta_d| = 1$. Only the excitation spectrum of the edge modes located on *one* boundary is plotted for clarity in all cases. Panel (a): $h_z = 0, \epsilon = 0$. A pair of gapless Majorana modes exist, with TR-partners counterpropagating along the boundary. Panel (b): $h_z = 0, \epsilon = 0.2$. Due to the phase mismatch, the helical edge modes becomes gapped [compare to Fig. 11(top)]. Panel (c) $h_z = 0.2, \epsilon = 0.2$. Gapped helical edge modes still exist with asymmetric bulk excitation spectrum for the counter-propagating modes. The bulk gap closes at $\epsilon = 0.2, h_z \approx 1.0$. Panel (d): $h_z = 1.5, \epsilon = 0.2$. A pair of gapless Majorana modes is restored, with both members propagating along the same direction along the boundary. System size: $(N_x, N_y) = (80, 100)$.

backscattering if only one mode is present on each edge). Thus, the robustness of edge modes ultimately depends on the specific form of the perturbations.

As implied by the above discussion, the application of a TR-breaking Zeeman magnetic field allows for effectively changing the helical nature of the original TR-invariant edge spectrum of H_D into a chiral one [Figs. 6 and 11]. In fact, the interplay between a phase mismatch in the pairing gaps and an applied Zeeman field may be exploited to steer the system across a topological QPT between helical and chiral phases. This is explicitly demonstrated in Fig. 12, where for clarity the edge modes propagating *only on one* boundary are plotted. Starting from a TS phase at $\epsilon = 0 = h_z$ supporting a Kramers' pair of helical Majorana modes [panel (a)], a non-zero phase mismatch causes these two modes to become gapped [panel (b)]. As a Zeeman field is turned on, both the edge and bulk spectrum are modified [panel (c)], until for a sufficiently strong field gapless Majorana modes are restored [panel (d)]. As in Fig. 11(top), there are still two Majorana modes, which travel in the same direction along each edge, thus forming a chiral pair. This helical-to-chiral transformation is accompanied by a closing of the bulk gap, which we have verified happens for parameter values intermediate between (c) and (d) [data not shown].

As noted in discussing Fig. 11(bottom), it is also possible that upon increasing the Zeeman magnetic field, one of the original Majorana modes dissolves into the bulk, leaving the system in a topologically non-trivial chiral phase. Interestingly, a topological QPT between a helical quantum spin Hall phase and a chiral spin-imbalanced quantum Hall state was also predicted in Ref. 55 for a 2D honeycomb fermionic lattice. While such a QPT is induced by tuning a Rashba SO coupling rather than a Zeeman field, our results point to suggestive similarities between the underlying physics and additional routes for topological phases manipulation.

V. CANDIDATE MATERIAL REALIZATIONS

Identifying superconducting materials for which the Hamiltonian H_D in Eq. (2), or its spin-singlet variant $\tilde{H}_D$ in Eq. (11), may provide an adequate physical model requires an in-depth dedicated study which is beyond our current scope. In this section, we nevertheless provide some perspective that may be useful to guide further exploration, also in the context of ongoing experiments.

At the time of writing, recently discovered materials such as $Cu_xBi_2Se_3$[34,36] and $Sn_{1-x}In_xTe$[35] are attracting significant attention as possible TR-invariant (centrosymmetric) TSs in 3D. In general, strongly SO-coupled doped semiconductors are natural candidates to search for topological superconductivity. The presence of a zero-bias conductance peak (ZBCP) in the measured point-contact spectrum has been interpreted, in particular, as a signature of the surface helical Majorana fermions associated with a non-trivial topological behavior. Experimentally, it is observed that such a ZBCP has a distinctive magnetic-field dependence, its amplitude being strongly suppressed by a relatively weak Zeeman field applied perpendicularly to the cleaved surface, consistent with delocalization of Majorana modes[58]. While a theoretical description of $Cu_xBi_2Se_3$ has been proposed based on an unconventional *spin-triplet pairing with odd parity*[25,59], scanning tunneling spectroscopy measurements of the superconducting gap appear to be consistent, at least for current Cu concentration, with a fully gapped s-wave spectrum and no mid-gap energy state[36].

With reference to our two-band model, there are two aspects we would like to highlight in regard to the above discussion. First, we have investigated the density of Majorana modes (*DMM*) on the boundary as a function of the magnetic field strength in both 2D and 3D. Suppose, specifically, that the system is originally in a TS phase characterized by CNs $(C_+^0, C_+^\pi) = (1, 0)$ in 3D and $C_+ = 1$ in 2D, in which cases a TR-pair of Majorana modes at the Dirac cones exist on each edge. When a weak magnetic field is applied, such that TR is broken

but the CNs remain unchanged, the two Majorana modes become a quasi-TR-pair and may thus be expressed as in Eq. (26). Therefore, the *DMM* on a given boundary (say, $j_y = 1$) may be computed as

$$DMM = \left(\left|\tilde{\alpha}_1\right|^2 + \left|\tilde{\beta}_1\right|^2 + \left|\tilde{\alpha}'_1\right|^2 + \left|\tilde{\beta}'_1\right|^2 \right), \qquad (27)$$

with an equivalent definition holding for the other boundary. The numerically computed *DMM* in 2D (3D) is shown in the main (inset) panels of Fig. 13, respectively. Clearly, in our two-band TS, a weak applied magnetic field delocalizes the Majorana fermions in both cases, qualitatively similar to the observed ZBCP dependence.

Second, it is interesting to contrast the *DMM* behavior to the one of a quantity which is more directly related to the measured scanning-tunneling spectrum, namely, the local density of states (LDOS), computed as

$$LDOS(j_y,E) = \frac{1}{N_x} \sum_{n,k_x} \sum_{i=1,4} \Big[\left|u_i(n,k_x,j_y)\right|^2 \delta(E-\epsilon_{n,k_x}) + \left|v_i(n,k_x,j_y)\right|^2 \delta(E+\epsilon_{n,k_x}) \Big], \qquad (28)$$

where $(u_1,\ldots,u_4,v_1,\ldots,v_4)^\dagger$ is the single-particle eigenvector corresponding to energy ϵ_{n,k_x} of $H_D + H_M^{(z)}$ with PBC in the $\hat{x}$ direction, and OBC in the $\hat{y}$ direction. While a more in-depth analysis will be presented elsewhere[60], numerical results for the *LDOS* profile of the same 2D TS considered in Fig. 13 are shown in Fig. 14, for selected values of the applied Zeeman field. Despite the existence of zero-energy Majorana modes in the fully gapped TS under consideration, no peak is manifest at zero energy (unlike in 1D[58]). Although the absence of such a peak is consistent with the measurements in Ref. 36, our *DMM* and *LDOS* results taken together suggest that care is needed in diagnosing the presence or absence of Majorana modes from such quantities, as also remarked in Ref. 34. A conclusive determination will likely require additional cross-checks, including spectroscopic measurements on higher doped materials. Confirmation of the absence of a zero-energy peak, along with evidence for spin-singlet pairing and/or of a two-gap behavior would constitute experimental signatures in favor of our TS model in describing these or possibly similar doped-semiconducting materials.

A different intriguing possibility is provided by s-wave pairing with a sign reversal of the superconducting order parameter between different Fermi surface sheets, resulting in so-called $s_\pm$ *symmetry*[61,62]. While an unambiguous experimental characterization has yet to be established, $s_\pm$ symmetry is widely believed to be realized and play an important role in iron-based superconductors of both the iron-pnictide and the chalcogen-based family[29]. Interestingly, for such superconductors, it has been experimentally established that the Cooper pairs consist of spin singlets, and their $s_\pm$ symmetry would automatically realize the π-symmetry condition that is required for our TR-invariant Hamiltonian to support non-trivial topological

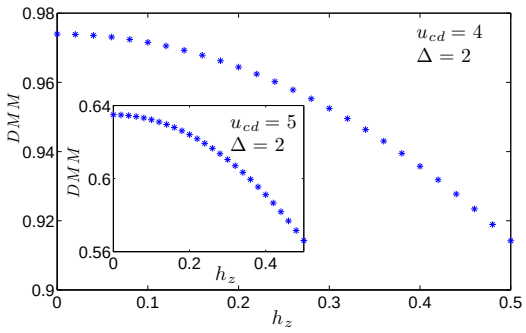

FIG. 13: (Color online) Density of Majorana modes on the boundary [Eq. (27)] for the 2D (main panel) and 3D (inset) Hamiltonian $H_D + H_M^{(z)}$ as a function of the applied magnetic field strength h_z, and $\mu = -1$. System size: $(N_x, N_y) = (40, 100)$ for 2D, and $(N_x, N_y, N_z) = (40, 100, 40)$ for 3D.

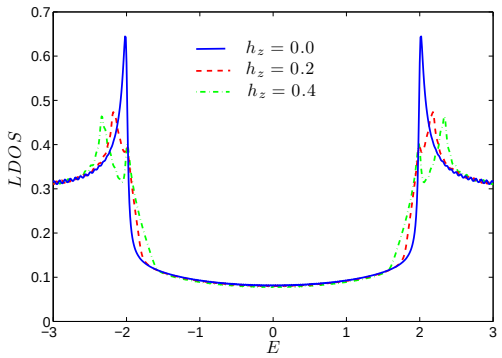

FIG. 14: (Color online) Local density of states on the boundary [$j_y = 1$, Eq. (28)] for the 2D Hamiltonian $H_D + H_M^{(z)}$ for different values of the applied magnetic field strength h_z. The remaining parameters are the same as in Fig. 13, except the system size is now $(N_x, N_y) = (400, 80)$.

phases and Majorana modes to emerge. Although additional quantitative study is certainly needed before any solid conclusion can be reached (see also Ref. 63 for a recent proposal on topological superconductivity via proximity effects between $s_\pm$ wave iron-based superconductor and semiconductors), we conjecture that iron-based materials may provide a natural candidate for realizing our model in Nature, as first suggested in Ref. 30.

VI. CONCLUSIONS

We have continued our investigation of *time-reversal invariant multiband s-wave topological superconductors* as introduced in Ref. 30. This class of superconductors involves at least two spin-1/2 fermionic bands, spin-orbit coupling, and bulk s-wave superconducting fluctuations. In the two-band case, provided that a *sign reversal* (π shift) between the superconducting pairing gaps is realized, the model can be analytically solved in 1D, 2D, and

3D upon restricting to the excitation spectrum of time-reversal invariant momentum modes. Our model may then be interpreted as either an intra-band or an inter-band *spin-singlet bulk topological superconductor*, since there exists an exact unitary mapping connecting both representations. From the standpoint of the classification introduced in Ref. 39, our model belongs to the DIII symmetry class, as shown in full mathematical detail in Appendix A. In the absence of superconductivity our Hamiltonian describes a topological insulator, and thus one may think of our superconducting state as emerging from a doped topological insulator.

An important part of our work is the topological characterization, into trivial as opposed to non-trivial topological states, of the various possible phases generated as a result of changes in the parameters of our model Hamiltonian. To this end, we have introduced (and explained in Appendix D how to numerically compute) corresponding bulk $\mathbb{Z}_2$ topological invariants that are, in principle, generalizable to interacting systems. In the time-reversal invariant case, only one Kramers' sector is included in the computation of the topological invariants, while when TR symmetry is explicitly broken we have showed how to modify these bulk topological invariants to include all the states. Physically, these topological invariants are key to understanding the bulk-boundary correspondence between the (trivial and non-trivial) topological nature of the bulk state and the existence of robust Majorana edge modes. Topologically non-trivial superconducting phases support an odd number of Kramers' pairs (in the time-reversal-invariant case) or an odd number (in the broken time-reversal case) of Majorana modes on each boundary, respectively. Topologically non-trivial phases are associated to robust Majorana edge states: in the time-reversal-invariant case they are robust against perturbations that preserve such symmetry, while in the broken time-reversal symmetry case they are robust against different kinds of perturbations.

Throughout this work, emphasis has been put into exploring: (1) the relation between the spatial dimensionality of our model and the emergence of non-trivial topological phases; and (2) the stability/robustness of gapless Majorana edge states under different mechanisms for breaking time-reversal symmetry, such as applied or impurity magnetic fields or broken time-reversal invariance due to a deviation from $\pi-$shifted superconducting gaps. While a number of interesting problems remain open for further investigation as indicated in the text, our main findings may be itemized as follows:

- Nontrivial topological phases that exists in our 2D two-band time-reversal invariant model[30] can be extended to 1D and 3D. Topologically trivial and non-trivial s-wave spin-singlet superconducting phases exist in all the spatial dimensions studied;
- Lower-dimensional $\mathbb{Z}_2$ invariant can be extended to characterize higher dimensional topological phases;
- Gapless pairs of Majorana modes that exist in a topologically non-trivial phase in the absence of an applied or impurity magnetic field may remain gapless under such a perturbation. However, since these Majorana modes are no longer protected by time-reversal symmetry, their degree of robustness against subsequent perturbations is, in general, different as compared to the original Kramers' pairs, and dependent upon the perturbation details;
- Suitable static magnetic fields may be used to restore Majorana edge modes when the phase of the gaps of the superconductor is not π-shifted;
- Under the effect of a Zeeman magnetic field, helical Majorana excitations in our time-reversal invariant model may be transformed into chiral Majorana excitations, providing an interesting example of a topological quantum phase transition;
- Candidate materials that may potentially realize our proposal for time-reversal invariant topological superconductivity and Majorana edge modes may be provided by strongly spin-orbit coupled doped semiconductors or iron-based superconductors with $s_\pm$ pairing symmetry.
- The existence of Majorana edge modes in 2D (and 3D) fully gapped TS need not imply a zero-energy peak in the local density of states on the surface. Thus, care is needed in interpreting point-contact and scanning-tunneling spectroscopy measurements and in identifying unambiguous experimental signatures.

Acknowledgements

It is a pleasure to thank B. Seradjeh, A. W. W. Ludwig and S. Ryu for useful input and correspondence. Support from the NSF through Grant No. PHY-0903727 (to LV) is gratefully acknowledged.

[1] H. Nishimori and G. Ortiz, *Elements of Phase Transitions and Critical Phenomena* (Oxford University Press, Oxford, 2011).
[2] A. Y. Kitaev, Ann. Phys. **321**, 2 (2003).
[3] C. Nayak *et al.*, Rev. Mod. Phys. **80**, 1083 (2008).
[4] C. L. Kane and E. J. Mele, Phys. Rev. Lett. **95**, 146802 (2005).
[5] M. Z. Hasan and C. L. Kane, Rev. Mod. Phys. **82**, 3045 (2010).
[6] N. Read and D. Green, Phys. Rev. B **61**, 10267 (2000).
[7] D. A. Ivanov, Phys. Rev. Lett. **86**, 268 (2001).
[8] A. Y. Kitaev, Phys. Uspekhi **44**, 131 (2001).
[9] X. L. Qi, and S. C. Zhang, Rev. Mod. Phys. **83**, 1057 (2011).
[10] E. Majorana, Nuovo Cimento **14**, 171 (1937).
[11] G. Moore and N. Read, Nucl. Phys. B **360**, 362 (1991).
[12] F. Wilczek, Nature Phys. **5**, 614 (2009).
[13] R. M. Lutchyn *et al.*, Phys. Rev. Lett. **105**, 077001 (2010);

ibid. **106**, 127001 (2011); R. M. Lutchyn and M. A. Fisher, Phys. Rev. B **84**, 214528 (2011).
[14] Y. Oreg, G. Refael, and F. von Oppen, Phys. Rev. Lett. **105**, 177002 (2010).
[15] A. C. Potter and P. A. Lee, Phys. Rev. Lett. **105**, 227003 (2010); A. C. Potter and P. A. Lee, Phys. Rev. B **83**, 094525 (2011).
[16] J. D. Sau, R. M. Lutchyn, S. Tewari, and S. Das Sarma, Phys. Rev. Lett. **104**, 040502 (2010); J. Alicea, Phys. Rev. B **81**, 125318 (2010).
[17] B. Zhou and S.-Q. Shen, Phys. Rev. B **84**, 054532 (2011).
[18] P. W. Brouwer, M. Duckheim, A. Romito, and F. V. Oppen, Phys. Rev. B **84**, 144526 (2011).
[19] S. B. Chung, H. J. Zhang, X. L. Qi, and S. C. Zhang, Phys. Rev. B **84**, 060510 (R) (2011).
[20] L. Fu and C. L. Kane, Phys. Rev. Lett. **100**, 096407 (2008).
[21] T. D. Stanescu, J. D. Sau, R. M. Lutchyn, and S. D. Sarma, Phys. Rev. B **81**, 241310(R) (2010).
[22] B. A. Volkov and O. A. Pankratov, JETP Lett. **42**, 178 (1985); O. A. Pankratov, S. V. Pakhomov, and B. A. Volkov, Solid State Commun. **61**, 93 (1987).
[23] X.-L. Qi *et al.*, Phys. Rev. Lett. **102**, 187001 (2009).
[24] M. Sato, Phys. Rev. B **81**, 220504(R) (2010).
[25] L. Fu, and E. Berg, Phys. Rev. Lett. **105**, 097001 (2010).
[26] H. Suhl, B. T. Matthias, and L. R. Walker, Phys. Rev. Lett. **3**, 552 (1959).
[27] J. Nagamatsu *et al.*, Nature **410**, 63 (2001).
[28] R. Khasanov *et al.*, Phys. Rev. Lett. **98**, 057007 (2007); M. Jourdan, A. Zakharov, M. Foerster, and H. Adrian, *ibid.* **93**, 097001 (2004); Y. Kamihara,T. Watanabe, M. Hirano, and H. Hosono, J. Am. Chem. Soc. **130**, 3296 (2008); A. P. Petrović *et al.*, Phys. Rev. Lett. **106**, 017003 (2011); T. Hanaguri, S. Niitaka, K. Kuroki, H. Takagi, Science **328**, 474 (2010).
[29] I. I. Mazin, Nature **464**, 183 (2010).
[30] S. Deng, L. Viola, and G. Ortiz, Phys. Rev. Lett. **108**, 036803 (2012).
[31] S. Nakosai, Y. Tanaka, and N. Nagaosa, Phys. Rev. Lett. **108**, 147003 (2012).
[32] B. Seradjeh, Phys. Rev. B **86**, 121101(R) (2012).
[33] As noted in Ref. 30, interpreting the band index as a layer index also allows to establish a *formal* similarity with Fu & Kane's proposal[20]. While the physics underlying the two models differ significantly, a phase difference of π between the pairing gaps of neighboring s-wave superconductors is also required in order for the corresponding junction to support Majorana fermions (in 1D) or, more generally, Majorana bound states.
[34] S. Sasaki *et al.*, Phys. Rev. Lett. **107**, 217001 (2011).
[35] S. Sasaki *et al.*, arXiv:1208.0059.
[36] N. Levy *et al.*, arXiv:1211.0267.
[37] G. Rosenberg and M. Franz, Phys. Rev. B **82**, 035105 (2010).
[38] L. Isaev, Y. H. Moon, and G. Ortiz, Phys. Rev. B **84**, 075444 (2011).
[39] A. Altland, and M. R. Zirnbauer, Phys. Rev. B **55**, 1142 (1997).
[40] R. Roy, New J. Phys. **12** 065009 (2010).
[41] L. Fu and C. L. Kane, Phys. Rev. B **74**, 195312 (2006).
[42] R. Roy, Phys. Rev. B **79**, 195322 (2009).
[43] G. Ortiz, and R. M. Martin, Phys. Rev. B **49**, 14202 (1994).
[44] G. Ortiz, P. Ordejón, R. M. Martin, and G. Chiappe, Phys. Rev. B **54**, 13515 (1996).
[45] M. V. Berry, Proc. R. Soc. Lond., **A392**, 45 (1984).
[46] J. Zak, Phys. Rev. Lett. **62**, 2747 (1989).
[47] E. Lieb, T. Schultz, and D. Mattis, Ann. Phys. (N.Y.) **16**, 407 (1961).
[48] Y. Niu *et al.*, Phys. Rev. B **85**, 035110 (2012).
[49] S. Ryu, A. P. Schnyder, A. Furusaki, and A. W. W. Ludwig, New J. Phys. **12**, 065010 (2010).
[50] A. Kubasiak, P. Massignan, and M. Lewenstein, EPL **92**, 46004 (2010).
[51] L. Fidkowski and A. Kitaev, Phys. Rev. B **81**, 134509 (2010).
[52] D. Hsieh *et al.*, Nature **452**, 970 (2008); D. Hsieh *et.al.*, Science **323**, 919 (2009); P. Roushan *et al.*, Nature **460**, 1106 (2009).
[53] Y. Yang *et al.*, Phys. Rev. Lett. **107**, 066602 (2011).
[54] Q. Liu *et al.*, Phys. Rev. Lett. **102**, 156603 (2009).
[55] N. Goldman, W. Beugeling, and C. Morais Smith, Europhys. Lett. **97**, 23003 (2012).
[56] T. Paananen and T. Dahm, arXiv:1210.4422.
[57] M. Sato, Y. Takahashi, and S. Fujimoto, Phys. Rev. Lett. **103**, 020401 (2009).
[58] J. D. Sau, S. Tewari, R. M. Lutchyn, T. D. Stanescu, and S. D. Sarma, Phys. Rev. B **82**, 214509 (2010).
[59] T. H. Hsieh and L. Fu, Phys. Rev. Lett. **108**, 107005 (2012).
[60] S. Deng, G. Ortiz, and L. Viola, "Majorana flat bands in s-wave gapless topological superconductors," forthcoming.
[61] I. I. Mazin, D. J. Singh, M. J. Johannes, and M. D. Hu, Phys. Rev. Lett. **101**, 057003 (2008).
[62] K. Ishida, Y. Nakai, and H. Hosono, J. Phys. Soc. Jpn. **78**, 062001 (2009).
[63] F. Zhang, C. L. Kane, and E. J. Mele, arXiv:1212.4232.

Appendix A: Symmetry class

Here, we provide an explicit representation of the discrete symmetry properties of our basic Hamiltonian, Eq. (2), as relevant to the topological classification of Refs. 39,49. In addition, we describe the hidden discrete symmetry mentioned in Sec. III B.

In second-quantized language, we define a anti-unitary TR operator $\mathcal{T}$, with $\mathcal{T}^2 = -I$, through its action on the fermion creation and annihilation operators. Specifically, let $\mathcal{T} \equiv U_T K$, where U_T and K are a unitary operator and complex conjugation, respectively, such that

$$\mathcal{T}(A_{\mathbf{k}})_j \mathcal{T}^{-1} \equiv \sum_l (U_T)_{jl} (A_{-\mathbf{k}})_l, \tag{A1}$$

where $(A_{\mathbf{k}})_j$ is the jth component of the vector $A_{\mathbf{k}}$ given after Eq. (4) in the main text. Thus, if we define

$$U_T = I_{4\times 4} \otimes i\sigma_y,$$

then the above condition yields

$$\mathcal{T} c(d)_{\mathbf{k},\uparrow} \mathcal{T}^{-1} = c(d)_{-\mathbf{k},\downarrow}, \;\; \mathcal{T} c^\dagger (d^\dagger)_{\mathbf{k},\downarrow} \mathcal{T}^{-1} = -c^\dagger (d^\dagger)_{-\mathbf{k},\uparrow},$$

$$\mathcal{T} c(d)_{\mathbf{k},\downarrow} \mathcal{T}^{-1} = -c(d)_{-\mathbf{k},\uparrow}, \;\; \mathcal{T} c^\dagger (d^\dagger)_{\mathbf{k},\uparrow} \mathcal{T}^{-1} = c^\dagger (d^\dagger)_{-\mathbf{k},\downarrow}.$$

Recall that $H_D = (1/2)\sum_{\mathbf{k}}(\hat{A}^\dagger_{\mathbf{k}}\hat{H}_{\mathbf{k}}\hat{A}_{\mathbf{k}} - 4\mu)$, where the single-particle Hamiltonian $\hat{H}_{\mathbf{k}}$ is given in Eq. (5). Direct calculation then yields

$$U_T^\dagger \hat{H}^*_{\mathbf{k}} U_T = \hat{H}_{-\mathbf{k}}. \tag{A2}$$

Accordingly, satisfying the requirement of TR symmetry [cf. Eq. (3) in Ref. 49 in momentum space].

Similarly, let us define an anti-unitary PH operator $\mathcal{C}$, with $\mathcal{C} \equiv U_C K$ and $\mathcal{C}^2 = +I$, through its action on the fermion creation and annihilation operators, where U_C is a unitary operator, such that

$$\mathcal{C}(A_{\mathbf{k}})_j \mathcal{C}^{-1} = \sum_l (U_C)_{jl}(A_{-\mathbf{k}})_l. \tag{A3}$$

Thus, if we define U_C as

$$U_C = \sigma_x \otimes I_{4\times 4},$$

it follows that

$$\mathcal{C}d(c)_{\mathbf{k},\sigma}\mathcal{C}^{-1} = d^\dagger(c^\dagger)_{\mathbf{k},\sigma}, \quad \mathcal{C}d^\dagger(c^\dagger)_{\mathbf{k},\sigma}\mathcal{C}^{-1} = d(c)_{\mathbf{k},\sigma}.$$

Direct calculation then yields

$$U_C^\dagger \hat{H}^*_{\mathbf{k}} U_C = -\hat{H}_{-\mathbf{k}} \tag{A4}$$

satisfying the requirement of PH symmetry in the single-particle representation [cf. Eq. (4) in Ref. 49 in momentum space]. In addition, it is also straightforward to verify that H_D also possesses a unitary inversion symmetry [cf. Eq. (C.29) in Ref. 49],

$$U_I^\dagger \hat{H}_{\mathbf{k}} U_I = \hat{H}_{-\mathbf{k}}, \tag{A5}$$

where the inversion operator may be expressed as

$$U_I = \sigma_z \otimes \sigma_x \otimes I_{2\times 2},$$

independently of the system's dimension D.

Interestingly, besides exhibiting the above manifest discrete symmetries, our Hamiltonian may also preserve additional accidental "hidden" symmetries. While a characterization is far from trivial, we have explicitly identified one such $\mathbb{Z}_2 \otimes \mathbb{Z}_2 \otimes \mathbb{Z}_2 \otimes \mathbb{Z}_2$ symmetry in the limit where $\mu = 0, \lambda = t$. In order to describe this symmetry, let us now introduce the following new canonical Dirac fermion operators:

$$\begin{cases} \tilde{a}_{j,\uparrow} = \frac{1}{2}(c_{j,\uparrow} + d_{j,\uparrow} + c^\dagger_{j,\downarrow} - d^\dagger_{j,\downarrow}), \\ \tilde{b}_{j,\uparrow} = \frac{1}{2}(c_{j,\uparrow} + d_{j,\uparrow} - c^\dagger_{j,\downarrow} + d^\dagger_{j,\downarrow}), \\ \tilde{a}_{j,\downarrow} = \frac{1}{2}(c_{j,\downarrow} + d_{j,\downarrow} + c^\dagger_{j,\uparrow} - d^\dagger_{j,\uparrow}), \\ \tilde{b}_{j,\downarrow} = \frac{1}{2}(c_{j,\downarrow} + d_{j,\downarrow} - c^\dagger_{j,\uparrow} + d^\dagger_{j,\uparrow}), \end{cases}$$

which actually take a simpler form once expressed in terms of the a and b fermion operators defined in Eq. (7):

$$\begin{cases} \tilde{a}_{j,\uparrow} = \frac{1}{\sqrt{2}}(a_{j,\uparrow} + b^\dagger_{j,\downarrow}), \\ \tilde{b}_{j,\uparrow} = \frac{1}{\sqrt{2}}(a_{j,\uparrow} - b^\dagger_{j,\downarrow}), \\ \tilde{a}_{j,\downarrow} = \frac{1}{\sqrt{2}}(a_{j,\downarrow} + b^\dagger_{j,\uparrow}), \\ \tilde{b}_{j,\downarrow} = \frac{1}{\sqrt{2}}(a_{j,\downarrow} - b^\dagger_{j,\uparrow}). \end{cases} \tag{A6}$$

Upon expressing the Hamiltonian H_D, with $\mu = 0$ and $\lambda = t$, in terms of the newly defined fermion operators $\tilde{a}_{j,\sigma}$, $\tilde{b}_{j,\sigma}$, the following commutation relationships are found to hold:

$$\left[H_{D=1}, \bigotimes_{\sigma,\tilde{c}} \left(e^{i\pi \sum_j \tilde{c}^\dagger_{j,\sigma}\tilde{c}_{j,\sigma}}\right)\right] = 0,$$

$$\left[H_{D=2}, \bigotimes_{\sigma,\tilde{c}} \left(e^{i\pi \sum_{j_y} \tilde{c}^\dagger_{k_x,c,j_y,\sigma}\tilde{c}_{k_x,c,j_y,\sigma}}\right)\right] = 0,$$

$$\left[H_{D=3}, \bigotimes_{\sigma,\tilde{c}} \left(e^{i\pi \sum_{j_y} \tilde{c}^\dagger_{k_x,c,j_y,k_z,c,\sigma}\tilde{c}_{k_x,c,j_y,k_z,c\sigma}}\right)\right] = 0,$$

where the products run over $\sigma = \uparrow, \downarrow$ and $\tilde{c} = \tilde{a}, \tilde{b}$.

Recall that in Sec. III B we have considered the fate of the Majorana edge modes under a boundary perturbation H_p in 3D, Eq. (20). Thus, it is important to determine whether the total Hamiltonian $H_D + H_p$ still belongs to the same symmetry class. To this purpose, it is convenient to imagine that H_p acts *both* on the surface and in the bulk, in which case we can equivalently work under PBC. Thus, in place of Eq. (20), we may consider

$$\begin{aligned} H'_p &= \sum_{\mathbf{k},\sigma} u_p (c^\dagger_{k_x,k_y,k_z,\sigma} c_{-k_x,k_y,-k_z,\sigma} \\ &+ d^\dagger_{k_x,k_y,k_z,\sigma} d_{-k_x,k_y,-k_z,\sigma}) + \text{H.c.} \\ &= \sum_{\mathbf{k},\sigma} u_p (\tilde{a}^\dagger_{k_x,k_y,k_z,\sigma} \tilde{b}_{-k_x,k_y,-k_z,\sigma} \\ &+ \tilde{b}^\dagger_{k_x,k_y,k_z,\sigma} \tilde{a}_{-k_x,k_y,-k_z,\sigma}) + \text{H.c.} + \text{const}, \end{aligned}$$

where in the last two lines we have rewritten the perturbation using the new canonical operators $\tilde{a}_{k,\sigma}, \tilde{b}_{k,\sigma}$, and const is a c-number. Due to H'_p, the dimension of the single-particle Hamiltonian matrix $\hat{H}_{\mathbf{k}}$ is now doubled (to 16×16), and the matrices U_T and U_C for the TR and PH symmetries need to be changed correspondingly, that is,

$$U'_T = I_{8\times 8} \otimes i\sigma_y, \quad U'_C = I_{2\times 2} \otimes \sigma_x \otimes I_{4\times 4},$$

respectively, and similarly for U'_I. It can then be verified that the new perturbed Hamiltonian *still* exhibits both TR and PH symmetry, that is, Eq. (A2), Eq. (A4), and Eq. (A5) still hold. However, the perturbation H_p (H'_p) *does break* the hidden symmetry shown above, for $D = 3$. Notice that when the perturbation acts on the surface only, the dimensions of U_T and U_C are changed accordingly, nevertheless the conclusion that the perturbation still conserves the basic manifest discrete symmetries remains true.

Appendix B: The role of self-consistency

Throughout most of the discussion in the main text, and in particular in obtaining the phase diagrams of Fig. 1 and Fig. 2, the superconducting pairing gap Δ has been treated as a *free* control parameter, tunable at will. In real systems, however, Δ can only be obtained

by minimizing self-consistently the total free energy. Let $V_{cc} = V_{dd} \equiv V > 0$ in Eq. (3) denote the effective attraction strength in each band, and assume that the π-symmetry condition is obeyed, $\Delta_c = -\Delta_d$. Then, in 2D and at zero temperature, this amounts to minimizing the many-body ground-state energy,

$$E_{\rm gs} = 2N_xN_y\frac{\Delta^2}{V} + \sum_{\mathbf{k}}(\epsilon_{1,\mathbf{k}} + \epsilon_{2,\mathbf{k}} - 2\mu),$$

where the first term represents the condensation energy, and similar expressions hold in 1D and 3D.

As shown in Ref. 30, for $D = 2$ all the topological phases identified in the non-self-consistent regime are found to be *stable* for suitable choices of the control parameters in the self-consistent phase diagram, although new features may also emerge [see Fig. 3 therein and related discussion]. It would be interesting to obtain a full self-consistent description without imposing that $V_{cc} = V_{dd}$ and $\Delta_c = -\Delta_d$, that is, by leaving the two pairing gaps as independent parameters to be determined separately for generic intra-band parameters, and also allowing for an inter-band scattering term $V_{cd} \neq 0$. While such a complete study is beyond our current scope, we have verified that, as long as Eq. (6) is obeyed, all the trivial and the non-trivial topological phases in both 1D and 3D remain physically accessible for suitable parameters after imposing the self-consistency constraint. In a similar spirit, self-consistent calculations have also been performed for representative parameter values in the presence of a magnetic field, as discussed in Sec. IV.

Appendix C: Explicit form of Hamiltonian matrices

Consider the most general case of 3D geometry, under the condition of π-shifted gaps, $\Delta_c = -\Delta_d = \Delta$. Recall that for general parameter values and PBC, the Hamiltonian matrix with respect to the operator basis $\{A_{\mathbf{k}}\}$ takes the form given in Eq. (5). Upon transforming to the fermionic operators $\{a_{\mathbf{k},\sigma}, b_{\mathbf{k},\sigma}\}$ defined in Eq. (7) and, for convenience, moving to the slightly different operator basis

$$\hat{B}'^{\dagger}_{\mathbf{k}} \equiv (a^{\dagger}_{\mathbf{k},\uparrow}, b^{\dagger}_{\mathbf{k},\downarrow}, a_{-\mathbf{k},\uparrow}, b_{-\mathbf{k},\downarrow}, a^{\dagger}_{\mathbf{k},\downarrow}, b^{\dagger}_{\mathbf{k},\uparrow}, a_{-\mathbf{k},\downarrow}, b_{-\mathbf{k},\uparrow}),$$

the new Hamiltonian matrix $\hat{H}'_{\mathbf{k}}$ becomes:

$$\hat{H}'_{\mathbf{k}} = \begin{pmatrix} -\mu + \lambda_{k_x}\sigma_x + \lambda_{k_y}\sigma_y + m_{\mathbf{k}}\sigma_z & i\Delta\sigma_y & i\lambda_{k_z}\sigma_y & 0 \\ -i\Delta\sigma_y & \mu + \lambda_{k_x}\sigma_x - \lambda_{k_y}\sigma_y - m_{\mathbf{k}}\sigma_z & 0 & i\lambda_{k_z}\sigma_y \\ -i\lambda_{k_z}\sigma_y & 0 & -\mu + \lambda_{k_x}\sigma_x - \lambda_{k_y}\sigma_y + m_{\mathbf{k}}\sigma_z & -i\Delta\sigma_y \\ 0 & -i\lambda_{k_z}\sigma_y & i\Delta\sigma_y & \mu + \lambda_{k_x}\sigma_x + \lambda_{k_y}\sigma_y - m_{\mathbf{k}}\sigma_z \end{pmatrix},$$

where as before we define $\vec{\lambda}_{\mathbf{k}} = -2\lambda\sum_{\nu\in u_D}\sin k_\nu \hat{e}_\nu \equiv (\lambda_{k_x}, \lambda_{k_y}, \lambda_{k_z})$, and $m_{\mathbf{k}} = u_{cd} - 2t\sum_{\nu\in u_D}\cos k_\nu$. The above expression makes it clear why, due to the SO component λ_{k_z}, a decoupled structure no longer arises in 3D for arbitrary momentum values.

In the presence of an applied magnetic field with components (h_x, h_y, h_z) as in Eq. (21), the general expression for the resulting Hamiltonian matrix of $H_D + H_M$ becomes:

$$\hat{H}''_{\mathbf{k}} = \begin{pmatrix} -\mu + \lambda_{k_x}\sigma_x + \lambda_{k_y}\sigma_y + m_{+,\mathbf{k}}\sigma_z & i\Delta\sigma_y & i\lambda_{k_z}\sigma_y + h_x - ih_y\sigma_z & 0 \\ -i\Delta\sigma_y & \mu + \lambda_{k_x}\sigma_x - \lambda_{k_y}\sigma_y - m_{+,\mathbf{k}}\sigma_z & 0 & i\lambda_{k_z}\sigma_y - h_x - ih_y\sigma_z \\ -i\lambda_{k_z}\sigma_y + h_x + ih_y\sigma_z & 0 & -\mu + \lambda_{k_x}\sigma_x - \lambda_{k_y}\sigma_y + m_{-,\mathbf{k}}\sigma_z & -i\Delta\sigma_y \\ 0 & -i\lambda_{k_z}\sigma_y - h_x + ih_y\sigma_z & i\Delta\sigma_y & \mu + \lambda_{k_x}\sigma_x + \lambda_{k_y}\sigma_y - m_{-,\mathbf{k}}\sigma_z \end{pmatrix},$$

where $m_{\pm,\mathbf{k}} \equiv m_{\mathbf{k}} \pm h_z$, as also defined in the main text. The above expression makes it clear that, when $k_z = k_{z,c} \in \{0, \pi\}$ ($\lambda_{k_z} = 0$), we may still obtain an analytical solution of the excitation spectrum for a magnetic field in the z direction, with respect to the above operator basis $\hat{B}'_{\mathbf{k}}$. Similarly, it is possible in principle to find a suitable basis (not shown) such that an analytical solution of the excitation spectrum exists for $k_\nu = k_{\nu,c}$, $\nu = x$ or y, in the presence of a magnetic field along the x or y direction, respectively.

Appendix D: Numerical evaluation of topological invariants

In numerical computations of topological invariants, it is crucial to guarantee that the results be *numerically gauge-invariant*[43,44], otherwise one gets non-sensical results because of the random phases generated from numerical diagonalization of H_D. We briefly describe here the procedure we followed to ensure numerical gauge-invariance.

Recall the definition of the Berry phase [Eq. (12)]:

$$B_n = i \int_{-\pi}^{\pi} dk \, \langle \psi_{n,k} | \partial_k \psi_{n,k} \rangle,$$

in terms of normalized states, $\langle \psi_{n,k} | \psi_{n,k} \rangle = 1$. The phase $\varphi(n,k,k')$ of the matrix element $\langle \psi_{n,k} | \psi_{n,k'} \rangle$ satisfies the following relation:

$$\begin{aligned} i \langle \psi_{n,k} | \partial_k \psi_{n,k} \rangle &= -\partial_{k'} \varphi(n,k,k')|_{k'=k} \\ &= -\partial_{k'} \big(\mathrm{Im} \ln \langle \psi_{n,k} | \psi_{n,k'} \rangle \big)|_{k'=k}, \end{aligned} \tag{D1}$$

where in the last line the definition of the phase $\varphi(n,k,k')$ was used. Then, the Berry phase can be rewritten as

$$B_n = -\int_{-\pi}^{\pi} dk \, \partial_{k'} \varphi(n,k,k')|_{k'=k},$$

admitting a simple discretized approximation[43,44]

$$\begin{aligned} B_n &= \lim_{N\to\infty} \sum_{i=0}^{N-1} \Delta\varphi(n,i,i+1), \\ &= -\lim_{N\to\infty} \mathrm{Im} \ln \prod_{i=0}^{N-1} \langle \psi_{n,k_i} | \psi_{n,k_{i+1}} \rangle, \end{aligned} \tag{D2}$$

with the identification of the states ($k_0 = -\pi, k_N = \pi$)

$$|\psi_{n,k_N}\rangle \equiv |\psi_{n,k_0}\rangle.$$

In practice one needs only a few (some tenths) points in the above product for a stable result to be found.

Similarly, the CN C_n is given by [Eq. (15)]:

$$C_n = \frac{1}{\pi} \int_{-\pi}^{\pi} dk_x \int_{-\pi}^{\pi} dk_y \, \mathrm{Im} \, \langle \partial_{k_x} \psi_{n,\mathbf{k}} | \partial_{k_y} \psi_{n,\mathbf{k}} \rangle.$$

In numerical computations of C_n, we approximate the integrand in Eq. (15) as

$$\begin{aligned} &\mathrm{Im} \, \langle \partial_{k_x} \psi_{n,\mathbf{k}} | \partial_{k_y} \psi_{n,\mathbf{k}} \rangle \approx \\ &\qquad \frac{1}{\epsilon^2} \mathrm{Im} \, [\ln(\langle \psi_{n,\mathbf{k}} | \psi_{n,\mathbf{k}_x} \rangle \langle \psi_{n,\mathbf{k}_x} | \psi_{n,\mathbf{k}_y} \rangle \langle \psi_{n,\mathbf{k}_y} | \psi_{n,\mathbf{k}} \rangle)], \end{aligned}$$

where $\mathbf{k}_\nu \equiv \mathbf{k} + \epsilon \hat{k}_\nu$, $\hat{k}_\nu$ are unit vectors in momentum space, and $\epsilon \ll 1$. Finally, we compute C_n as

$$C_n = \frac{1}{\pi} \mathrm{Im} \prod_{\mathbf{k}} \ln(\langle \psi_{n,\mathbf{k}} | \psi_{n,\mathbf{k}_x} \rangle \langle \psi_{n,\mathbf{k}_x} | \psi_{n,\mathbf{k}_y} \rangle \langle \psi_{n,\mathbf{k}_y} | \psi_{n,\mathbf{k}} \rangle)].$$